Denitrification, dehydration and ozone loss during the Arctic winter 2015/2016

Farahnaz Khosrawi[1], Oliver Kirner[2], Björn-Martin Sinnhuber[1], Sören Johansson[1], Michael Höpfner[1], Michelle L. Santee[3], Lucien Froidevaux[3], Jörn Ungermann[4], Roland Ruhnke[1], Wolfgang Woiwode[1], Hermann Oelhaf[1], and Peter Braesicke[1]

[1]Institute of Meteorology and Climate Research, Karlsruhe Institute of Technology, Karlsruhe, Germany
[2]Steinbuch Centre for Computing, Karlsruhe Institute of Technology, Karlsruhe, Germany
[3]Jet Propulsion Laboratory, California Institute of Technology, California, USA
[4]Institute of Energy and Climate Research, Forschungszentrum Jülich, Jülich, Germany

Correspondence to: Farahnaz Khosrawi (farahnaz.khosrawi@kit.edu)

Abstract. The Arctic winter 2015/2016 was one of the coldest stratospheric winters in recent years. A stable vortex formed by early December and the early winter was exceptionally cold. Cold pool temperatures dropped below the Nitric Acid Tri-hydrate (NAT) existence temperature of about 195 K, thus allowing polar stratospheric clouds (PSCs) to form. The low temperatures in the polar stratosphere persisted until early March allowing chlorine activation and catalytic ozone destruction. Satellite observations indicate that sedimentation of PSC particles led to denitrification as well as dehydration of stratospheric layers. Model simulations of the Arctic winter 2015/2016 nudged toward European Center for Medium-Range Weather Forecasts (ECMWF) analyses data were performed with the atmospheric chemistry-climate model ECHAM5/MESSy Atmospheric Chemistry (EMAC) for the Polar Stratosphere in a Changing Climate (POLSTRACC) campaign. POLSTRACC is a High Altitude and LOng Range Research Aircraft (HALO) mission aimed at the investigation of the structure, composition and evolution of the Arctic Upper Troposphere and Lower Stratosphere (UTLS). The chemical and physical processes involved in Arctic stratospheric ozone depletion, transport and mixing processes in the UTLS at high latitudes, PSCs as well as cirrus clouds are investigated. In this study an overview of the chemistry and dynamics of the Arctic winter 2015/2016 as simulated with EMAC is given. Further, chemical-dynamical processes such as denitrification, dehydration and ozone loss during the Arctic winter 2015/2016 are investigated. Comparisons to satellite observations by the Aura Microwave Limb Sounder (Aura/MLS) as well as to airborne measurements with the Gimballed Limb Observer for Radiance Imaging of the Atmosphere (GLORIA) performed on board of HALO during the POLSTRACC campaign show that the EMAC simulations nudged toward ECMWF analyses generally agree well with observations. We derive a maximum polar stratospheric O_3 loss of ~2 ppmv or 117 DU in terms of column ozone in mid March. The stratosphere was denitrified by about 4–8 ppbv HNO_3 and dehydrated by about 0.6–1 ppmv H_2O in mid to end of February. While ozone loss was quite strong, but not as strong as in 2010/2011, denitrification and dehydration were so far the strongest observed in the Arctic stratosphere in at least the past 10 years.

1 Introduction

Since the early eighties, thus for more than 30 years, substantial ozone depletion has been observed each year during winter and spring in the Antarctic stratosphere (WMO, 2010). Polar ozone depletion is associated with enhanced chlorine from anthropogenic chlorofluorocarbons and heterogeneous chemistry under cold conditions. The deep Antarctic "hole" contrasts with the generally weaker ozone depletion observed in the warmer Arctic (Solomon et al., 2014). Nevertheless, substantial ozone depletion has been observed for cold Arctic winters. Especially, in the past 15 years, ozone loss in the Arctic occasionally approached the degree of ozone loss in the Antarctic as in e. g. winter 2004/2005 (e.g. Manney et al., 2006; Tilmes et al., 2006; Livesey et al., 2015, and references therein) and 2010/2011 (e.g., Manney et al., 2011; Sinnhuber et al., 2011; Hommel et al., 2014).

Polar stratospheric clouds (PSCs) play a key role in stratospheric ozone destruction in the polar regions (Solomon et al., 1986; Crutzen and Arnold, 1986). Heterogeneous reactions which take place on and within the PSC particles convert halogens from relatively inert reservoir species into forms which can destroy ozone in the polar spring (e.g., Peter, 1997; Solomon, 1999; Lowe and MacKenzie, 2008). PSCs form at altitudes between 15–30 km and consist of liquid and/or solid particles. According to their composition and physical state they have been classified into three different types: (1) supercooled ternary solutions (STS), (2) Nitric Acid Trihydrate (NAT) and (3) water ice. Liquid PSC cloud particles (STS) form by the condensation of water vapour (H_2O) and nitric acid (HNO_3) on the liquid stratospheric background sulfate aerosol particles at temperatures 2–3 K below the NAT existence temperature T_{NAT} (~ 195 K at 50 hPa), while for the formation of solid cloud particles (NAT and ice) lower temperatures are required (slightly above or below the ice frost point $T_{ice} \sim 188$ K at 50 hPa) (e.g. Carslaw et al., 1994; Koop et al., 1995).

Solid PSC particles can grow to larger sizes than liquid PSC particles and finally sediment out of the stratosphere (Fahey et al., 2001). The sedimentation of the solid particles can lead to dehydration and/or denitrification of the stratosphere. Solid HNO_3 containing PSC particles leading to denitrification can either consist of NAT or ice depending on the prevailing formation mechanism. It has been shown that the nucleation of NAT on ice is quite efficient (e.g., Fueglistaler et al., 2002; Hoyle et al., 2013). The sedimentation of large HNO_3 containing ice PSC particles can lead to greater denitrification than the sedimentation of (typically smaller) NAT or liquid PSC particles alone (Lowe and MacKenzie, 2008; Wohltmann et al., 2013; Manney and Lawrence, 2016).

Denitrification limits the deactivation process of the ozone destroying substances in springtime and thus leads to a prolongation of the ozone destroying cycles (e.g., Salawitch et al., 1993; Rex et al., 1997). Evidence of denitrification has been found in the Arctic and Antarctic from in situ and remote sensing observations (Fahey et al., 1990; Solomon, 1999; Waibel et al., 1999; Kondo et al., 2000; Santee et al., 2000; Manney et al., 2011). Denitrification is most intense over the Antarctic region, where large fractions of available NO_y are irreversibly removed from the stratosphere each winter. NO_y is the sum of principal reactive nitrogen species, of which HNO_3, NO, NO_2, N_2O_5, and $ClONO_2$ are important in the lower stratosphere (Fahey et al., 1989). Dehydration in the stratosphere is generally observed over the Antarctic (e.g., Kelly et al., 1989; Vömel et al.,

1995; Nedoluha et al., 2000) but only rarely in the Arctic (e.g., Fahey et al., 1990; Vömel et al., 1997; Pan et al., 2002; Schiller et al., 2002; Khaykin et al., 2013).

Another factor contributing to the severity of polar ozone destruction is the reduction of nitrogen (NO_x=NO+NO_2) via the conversion of NO_x into HNO_3 on the surfaces of PSCs, the so-called denoxification. Denoxification becomes important if temperatures are continuously low during the course of the winter as is the case in the Antarctic (e. g. Waibel et al., 1999). It has been shown that polar vortex stability, chlorine activation and ozone loss tend to be greater with lower vortex temperatures (e. g. von Hobe et al., 2013). Therefore, it is not surprising that the most severe ozone loss ever observed in the Arctic occurred in spring 2011, at the end of the most persistently cold Arctic winter in the stratosphere on record (Manney et al., 2011; Sinnhuber et al., 2011; Hommel et al., 2014).

The Arctic winter 2015/2016 was one of the coldest stratospheric winters in recent years. Indeed, the Arctic polar vortex in the early winter 2015/2016 was the strongest and coldest of the last 68 years (Matthias et al., 2016). Temperatures within the vortex dropped below T_{NAT}, thus allowing PSCs to form. Tropospheric and stratospheric cloud structures were observed simultaneously over Svalbard. Synoptic-scale PSCs extended over a nearly $8\,km$ deep layer (Dörnbrack et al., 2017). The low temperatures in the polar stratosphere persisted until early March allowing PSC formation, chlorine activation and catalytic ozone destruction. Satellite observations indicate that sedimentation of PSC particles led to denitrification as well as dehydration of stratospheric layers (Manney and Lawrence, 2016). Widespread persistent ice PSC layers were observed by the Cloud-Aerosol Lidar and Infrared Pathfinder Satellite Observations (CALIPSO) (Voigt et al., 2016). Ozone destruction was strong, but not as strong as in 2010/2011, since a major final sudden stratospheric warming ended the Arctic winter 2015/2016 by early March (Manney and Lawrence, 2016).

Model simulations of the Arctic winter 2015/2016 nudged toward European Center for Medium-Range Weather Forecasts (ECMWF) analyses were performed with the atmospheric chemistry-climate model ECHAM5/MESSy Atmospheric Chemistry (EMAC) for the POLSTRACC (Polar Stratosphere in a Changing Climate) campaign. POLSTRACC was a HALO mission (High Altitude and LOng Range Research Aircraft) aiming at the investigation of the structure, composition and evolution of the Arctic Upper Troposphere Lower Stratosphere (UTLS). The chemical and physical processes involved in Arctic stratospheric ozone depletion, transport and mixing processes in the UTLS at high latitudes, PSCs as well as cirrus clouds were investigated. In this study, an overview of the chemistry and dynamics of the Arctic winter 2015/2016 as simulated with EMAC is given. Chemical-dynamical processes such as denitrification, dehydration and ozone loss will be investigated and comparisons to satellite observations by the Aura Microwave Limb Sounder (Aura/MLS) as well as to airborne measurements with the Gimballed Limb Observer for Radiance Imaging of the Atmosphere (GLORIA) performed onboard of HALO will be shown.

2 Model simulations and observations

2.1 EMAC

The ECHAM5/MESSy Atmospheric Chemistry (EMAC) model is a numerical chemistry and climate simulation system that includes sub-models describing tropospheric and middle atmosphere processes and their interaction with oceans, land and human influences (Jöckel et al., 2010). It uses the second version of the Modular Earth Submodel System (MESSy2) to link multi-institutional computer codes. The core atmospheric model is the 5th generation European Centre Hamburg general circulation model (ECHAM5, Roeckner et al. (2006). For the present study we applied EMAC (ECHAM5 version 5.3.02, MESSy version 2.52) in T106L90MA and T42L90MA resolution, i.e., with a spherical truncation of T106 and T42 (corresponding to a quadratic Gaussian grid of approximately $1.125° \times 1.125°$ and $2.8° \times 2.8°$ degrees, respectively, in latitude and longitude) with 90 vertical hybrid pressure levels from the surface up to $0.01\,\mathrm{hPa}$ (approx. $80\,\mathrm{km}$). A Newtonian relaxation technique of the prognostic variables temperature, vorticity, divergence and the (logarithm of the) surface pressure above the boundary layer and below $1\,\mathrm{hPa}$ towards ECMWF ERA-Interim reanalysis data (Dee et al., 2011) and ECMWF operational analysis was applied, respectively, in order to nudge the model dynamics towards the observed meteorology.

For the analyses of the Arctic winter 2015/2016 we use the EMAC data from a T106L90 simulation that was chemically initialised based on a former EMAC simulation. The T106L90 simulation was started on 1 July 2015 and continued until 30 April 2016, applying a nudging toward ECMWF operational analysis. For the comparisons to recent winters we performed an EMAC T42L90 simulation covering the time period 1 January 2008 to 30 April 2016. The T42L90 simulation was nudged toward ECMWF ERA-interim analysis data until 30 June 2015 and toward ECMWF operational analysis data thereafter. In both simulations (T106L90 and T42L90) a comprehensive chemistry setup for the stratosphere and troposphere is included. Reaction rate coefficients for gas phase reactions and absorption cross sections for photolysis are taken from Atkinson et al. (2007) and Sander et al. (2011b). The applied model setup comprised among others the submodels: MECCA for the gas-phase chemistry (Sander et al., 2011a), JVAL for the calculation of photolysis rates (Sander et al., 2014), MSBM (Multi-phase Stratospheric Box Model) for the processes related to PSCs (Kirner et al., 2011), TROPOP for diagnosing the tropopause and boundary layer height, SORBIT for sampling model data along sun-synchronous satellite orbits (Jöckel et al., 2010) as well as H2O for stratospheric water vapor.

The submodel MSBM simulates the number densities, mean radii and surface areas of sulphuric acid aerosols and liquid and solid PSC particles. The formation of STS particles is calculated according to Carslaw et al. (1995) through the uptake of HNO_3 and H_2O on the liquid binary sulphuric acid/water particles. Ice particles are assumed to form homogeneously at temperatures below T_{ice}. For the simulation of NAT particles the "kinetic growth NAT parameterisation" is used. The "kinetic" parameterisation is based on the growth and sedimentation algorithm given by Carslaw et al. (2002) and van den Broek et al. (2004). The vapour pressure over ice is calculated according to Marti and Mauersberger (1993) and the vapour pressure over NAT according to Hanson and Mauersberger (1988). NAT formation takes place as soon as a supercooling of $3\,\mathrm{K}$ below T_{NAT} is reached. The sedimentation of ice particles is calculated according to Waibel et al. (1999) and for NAT particles according

4

to Carslaw et al. (2002). Eleven heterogeneous reactions that occur on the surfaces of liquid and solid PSC particles are considered. A comprehensive description of the submodel MSBM can be found in Kirner et al. (2011).

2.2 Aura/MLS

The Microwave Limb Sounder (MLS) on the Earth Observing System Aura Satellite was launched in July 2004. The Aura/MLS
5 instrument is an advanced successor to the MLS instrument on the Upper Atmosphere Research satellite (UARS). MLS is a limb sounding instrument that measures the thermal emission at millimetre and submillimetre wavelengths using seven radiometers to cover five broad spectral regions (Waters et al., 2006). Measurements are performed from the surface to $90\,\mathrm{km}$ with a global latitude coverage from $82°\,\mathrm{S}$ to $82°\,\mathrm{N}$. Vertical profiles are measured every $165\,\mathrm{km}$ along the suborbital track with a horizontal resolution of $\sim$200–500 km along track and a footprint of $\sim$3–9 km across-track. Here, we use Aura/MLS version v4.2 HNO_3,
10 O_3 and ClO data. The data screening criteria given by Livesey et al. (2017) have been applied to the data.

A detailed assessment of the quality and reliability of the Aura/MLS v2.2 HNO_3 measurements can be found in Santee et al. (2007). The HNO_3 in v3.3 was significantly improved compared to v2.2. In particular, the low bias in the stratosphere was largely eliminated. Measurements of v4.2 HNO_3 are performed with a horizontal resolution of 400–500 km and a vertical resolution of 3–4 km over most of the vertical range. In the lower stratosphere, the precision has been estimated to be 0.6 ppbv
15 and the systematic uncertainty for HNO_3 is estimated to be 0.5–2 ppbv (2-σ estimates) (Livesey et al., 2017).

Detailed validation of the MLS O_3 v2.2 product and comparisons with other data sets can be found in Jiang et al. (2007), Froidevaux et al. (2008) and Livesey et al. (2008). In the stratosphere and above, v4.2 ozone profiles are very similar to the v2.2 and v3.3x/v3.4x profiles. Comparisons have indicated general agreement within 5–10 % with stratospheric profiles from satellite, balloon, aircraft, and ground-based data (Livesey et al., 2017).

20 The quality and reliability of the v2.2 MLS ClO measurements were assessed in detail by Santee et al. (2008). The ClO product was significantly improved in v3.3 and v3.4 (Livesey et al., 2013). In particular, the substantial ($\sim$ 0.1–0.4 ppbv) negative bias present in the v2.2 ClO values at pressures larger than $22\,\mathrm{hPa}$ was mitigated to a large extent, primarily through retrieval of CH_3Cl, which was a new MLS product in v3.3 and v3.4. The ClO retrieval is largely unchanged over much of the profile in v4.2. Measurements of ClO are performed with a horizontal resolution of 300-600 km and a vertical resolution
25 of 3-4.5 km. The precision lies generally within ±0.1 ppbv (Livesey et al., 2017). Although the negative bias at the lowest retrieval levels has not been entirely eliminated, we make no attempt to correct for it in this analyses.

2.3 GLORIA

The Gimballed Limb Observer for Radiance Imaging of the Atmosphere (GLORIA) combines a classical Fourier transform spectrometer with a 2-D detector array. The instrument takes limb images of the atmosphere from the flight altitude of HALO
30 or M55-Geophysica down to $4\,\mathrm{km}$. This results in vertical sampling steps of about $150\,\mathrm{m}$ at $8\,\mathrm{km}$ tangent height from a typical HALO flight level of $14\,\mathrm{km}$. Individual images contain 128 pixels (spectra) in the vertical dimension and 48 pixels in the horizontal dimension. The spectra associated with the pixel rows are binned to reduce uncertainties. The spectral range of the observations currently extends from about 780 to $1400\,\mathrm{cm}^{-1}$ (Riese et al., 2014). The list of species with signatures in

this spectral range includes temperature, H_2O, HDO, O_3, CH_4, N_2O, CFC−11, CFC−12, HCFC−12, SF_6, HNO_3, N_2O_5, $ClONO_2$, HO_2NO_2, PAN, C_2H_6, H_2CO, NH_3. Details on the instrument design and calibration are given in Friedl-Vallon et al. (2014) and Kleinert et al. (2014). GLORIA is operated in a high-spectral, medium-spatial sampling ("chemistry") mode and a medium-spectral, high-spatial sampling ("dynamics") mode. The spectral samplings are $0.0625\,\mathrm{cm}^{-1}$ for the chemistry mode and $0.625\,\mathrm{cm}^{-1}$ for the dynamics mode (Riese et al., 2014). In this study, trace gas retrievals from measurements in the chemistry mode are used. A first validation of the retrieval results in the chemistry mode can be found in Woiwode et al. (2015).

3 Arctic winter 2015/2016

3.1 Overview

In the Arctic winter 2015/2016, temperatures were at record lows from December 2015 to early February 2016 with an unprecedented period of temperatures below the ice formation threshold (Manney and Lawrence, 2016). The extraordinarily strong and cold polar vortex in early winter (November-December 2015) was caused by very low planetary wave activity in the stratosphere (Matthias et al., 2016). The Arctic winter ended in early March by a major final sudden stratospheric warming. By mid-March, the vortex had been displaced far off the pole and split. The offspring vortices decayed rapidly, resulting in a full breakup of the vortex by early April (Manney and Lawrence, 2016).

In Fig. 1 the temporal evolution of temperature and PSC surface area density at high latitudes (70-90°N) as a function of pressure for December 2015 to March 2016 as simulated with EMAC is shown. Temperatures below $195\,\mathrm{K}$ are found between 70 and $10\,\mathrm{hPa}$ from early December to end of January. Zonal mean temperatures remained cold afterwards, but not as cold as during December and January. Temperatures dropped during the first cold period (December to end of January) below the ice formation threshold temperatures (Manney and Lawrence, 2016) leading to unprecedented formation of ice PSCs as will be discussed in more detail below (see Fig. 2). The simulated temperatures are in good agreement with observations from Aura/MLS (see Fig. 12 and Sect. 4.1).

The extensive formation of PSCs as simulated with EMAC can be seen in Fig. 1 (bottom). Here, the total surface area density (liquid + solid) is shown. The first PSCs are found in the beginning of December and PSC formation maximises throughout January (between 80 and $20\,\mathrm{hPa}$). During the second cold phase in February PSCs are still present but to a lesser extent. In Fig. 2 the surface area densities of STS, NAT and ice as a function of pressure are shown (70-90°N). Since the liquid particles have the largest surface area density, A_{STS} is almost identical to A_{PSC}. PSCs consisting of NAT are found between 150 and $20\,\mathrm{hPa}$ throughout December and January, and consisting of ice between 80 and $30\,\mathrm{hPa}$ in January. Compared to other extreme Arctic winters, e.g the 2010/2011 winter, much larger amounts of PSCs are simulated in accordance with the preceding low temperatures for the Arctic winter 2015/2016. Furthermore, the largest surface area density for ice is also simulated for the Arctic winter 2015/2016 as compared to previous Arctic winters e.g. the 2010/2011 Arctic winter, which has been the most extreme in that respective so far (e.g., Manney et al., 2011; Sinnhuber et al., 2011; Hommel et al., 2014). Ice PSCs persisted in

2015/2016 over a much longer time period than in e.g. the Arctic winter 2010/2011 as can be seen in the EMAC results for the Arctic winter 2010/2011 shown in Khosrawi et al. (2017).

3.2 Denitrification

Solid HNO_3 containing PSC particles can sediment out of the stratosphere and thus lead to an irreversible removal of HNO_3
5   (denitrification). Severe denitrification was observed by Aura/MLS in the Arctic winter 2015/2016. Figure 3 shows the HNO_3 gas phase distribution as simulated with EMAC for selected dates between 24 December 2015 and 12 February 2016 at $52\,\mathrm{hPa}$. Strong gas phase removal of HNO_3 is evident throughout the entire period considered here. Gas phase HNO_3 is extremely low within the Arctic vortex in December and January, but mixing ratios increase somewhat (but still remain quite low) in February. That this gas phase removal of HNO_3 led to a permanent removal and thus to a denitrification of the stratosphere can be seen
10   from the redistribution of NO_y in the model (Fig. 4).

In model simulations, denitrification can be quantified by applying a passive NO_y^* tracer. Figure 4 shows the simulated NO_y change (ΔNO_y) averaged over 70-90°N as function of pressure and time. The unperturbed NO_y^* was simulated by a passive tracer that was initialized according to the NO_y distribution on 1 December 2015. The passive tracer is transported as all other chemical species, but does not undergo any chemical changes or sedimentation. The difference of NO_y and NO_y^* gives the
15   amount of NO_y that has been denitrified/re-nitrified ($\Delta NO_y=NO_y-NO_y^*$).

Figure 4 shows that strong denitrification is also simulated with EMAC for the Arctic winter 2015/2016. The maximum sequestration is reached at the end of January (about $8\,\mathrm{ppbv}$). Below this layer re-nitrification (about $4\,\mathrm{ppbv}$) due to the evaporation of the sedimenting PSC particles at higher pressure levels (lower altitudes) is clearly visible. Thus, the amount of HNO_3 that has been permanently removed (denitrified) is between 4-8 ppbv. Diabatic descent within the polar vortex causes
20   the downward shift of the denitrified/re-nitrified areas.

3.3 Dehydration

The long period of temperatures below the ice formation threshold led to much greater dehydration than previously seen in the Arctic (Manney and Lawrence, 2016). Large areas of ice PSC throughout January were observed with CALIPSO that also were the greatest observed in the Arctic in the 8 years of the CALIPSO data record (Voigt et al., 2016). In the EMAC simulation
25   large areas of ice PSCs are simulated throughout January (Fig. 2 bottom). Dehydration peaks in the EMAC simulation towards the end of January and is also the strongest simulated compared to other cold winters as e.g. the Arctic winter 2010/2011. The simulated dehydration in EMAC is also in agreement with observations. Trace gas measurements from Aura/MLS show that exceptional dehydration occurred during the Arctic winter 2015/2016 (Manney and Lawrence, 2016).

Figure 5 shows the EMAC H_2O distribution at selected dates during the winter 2015/2016 at $52\,\mathrm{hPa}$. On 24 December 2015
30   the H_2O distribution shows the usual background H_2O mixing ratios in the Arctic region. From January onwards, mixing ratios drop and an area with mixing ratios below 5 ppmv is found north of Scandinavia. Mixing ratios decrease further throughout January and the area of dehydration increases. From February onwards H_2O mixing ratios start to increase again, but still remain lower than the pre-winter values.

Dehydration from the EMAC simulation is derived by using total "stratospheric" hydrogen ($2CH_4+H_2O$) as substitute for a passive H_2O tracer (e.g., Rinsland et al., 1996; Schiller et al., 1996). Molecular hydrogen (H_2) is nearly constant in the lower and middle stratosphere and can therefore be neglected in the calculation of total hydrogen. The quantity $2CH_4+H_2O$ is generally constant in the stratosphere. However, slight deviations from this quasi-conserved quantity can be found at high latitudes during winter where transport of mesospheric air rich in molecular hydrogen and poor in water vapour and methane is brought into the upper stratosphere (e.g., LeTexier et al., 1988; Engel et al., 1996).

The change in H_2O (ΔH_2O) is calculated by taking the difference of total hydrogen at time t and total hydrogen at time t_0 ($\Delta H_2O=(2CH_4+H_2O)(t)-(2CH_4+H_2O)(t_0)$, with $t_0 = 1$ December). The exceptional dehydration during the Arctic winter 2015/2016 can be seen in the temporal evolution of ΔH_2O as function of pressure averaged over 70-90°N (Fig. 6). The decrease of ΔH_2O throughout January and February shows a H_2O removal of around 1 ppmv extending between 60 and 30 hPa. Sequestration into PSC particles reaches its maximum in mid January (ΔH_2O of up to 2 ppmv). Below the depleted areas re-hydration (up to 0.6 ppmv) due to the evaporation of the sedimenting PSC particles at higher pressure levels (lower altitudes) is clearly visible. Thus, the amount of H_2O that has been permanently removed (dehydrated) is between 0.6-1ppmv.

3.4 Ozone loss

The Arctic winter 2015/2016 appeared to have the greatest potential yet seen for record Arctic ozone loss (Manney and Lawrence, 2016). Temperatures in the Arctic lower stratosphere were at record lows from December 2015 to early February 2016 (Manney and Lawrence, 2016; Matthias et al., 2016). As was shown by Manney and Lawrence (2016) ozone destruction began earlier and proceeded more rapidly than in 2010/2011, the winter that so far has been the one with the strongest observed ozone loss in the Arctic (Manney et al., 2011). That lower-stratospheric ozone loss did not reach the extent of that in spring 2011 was primarily due to a major final stratospheric warming in early March 2016 that led to a vortex split and a full breakdown of the vortex by early April (Manney and Lawrence, 2016).

In the following the EMAC simulation is used to investigate ozone depletion during the Arctic winter 2015/2016 and compare the results with previous Arctic winters. Ozone depletion (ΔO_3) from the model simulation is determined by the difference between the modelled ozone O_3 and a passive ozone tracer O_3^* ($\Delta O_3=O_3-O_3^*$). The passive ozone tracer was initialised on 1 December 2015 according to the ozone distribution on that day and was then advected and mixed as all other chemical species but did not undergo any chemical changes. The simulated ozone depletion (averaged over 70-90°N) is shown in Fig. 7. From mid January onwards ozone depletion is visible in the EMAC simulation and a maximum depletion of about 2.1 ppmv is reached at about 30 hPa in mid March.

The simulated total column ozone loss time series from 1 December to 31 March averaged over 70-90°N is shown in Fig. 8. Changes in the total column become visible from the end of January onwards. The absolute maximum in total column ozone loss of about 117 DU is reached on 7 March. Note that, rather than employing a vortex following coordinate as e. g. equivalent latitude, we haven chosen to perform our analyses on a fixed geographic latitude band. Such an approach is justified here because the use of a passive ozone tracer allows dynamical and chemical processes to be separated, thus facilitating the

quantification of chemical ozone loss. On equivalent latitudes the same amount of ozone loss in terms of mixing ratio is derived while in terms of column loss ozone loss is 10% less (103 DU).

3.5 Comparison to recent Arctic winters

The EMAC T42L90 simulation is used to compare the Arctic winter 2015/2016 to previous Arctic winters. The results from both simulations, T42L90 and T106L90, are quite similar as can be seen from the time series comparison shown in Section 4 where the EMAC simulations are compared to Aura/MLS observations. The agreement with the Aura/MLS measurements is slightly better for the T106L90 simulation.

Although considerable ozone loss occurred during the Arctic winter 2015/2016, ozone loss was not as strong as in 2010/2011 as can be seen from Fig. 9 and Fig. 10. In Fig. 9 the March mean O_3 column is shown for the years 2010 to 2016. Very low O_3 column values are found in March 2011. Column values reach 250 DU. In March 2016, however, the O_3 column remains quite high.

Figure 10 shows the Arctic mean column O_3 time series (averaged over $60°$ to $90°$N) from 1 December to 30 April for the four Arctic winters 2009/2010, 2010/2011, 2013/2014 and 2015/2016. The EMAC Arctic mean column O_3 shows considerable interannual variability. In contrast to the other Arctic winters, very low O_3 is found in 2010/2011. The extreme low O_3 column that we find in the EMAC simulation for the winter 2010/2011 is in agreement with the results from Strahan et al. (2013) and Manney et al. (2011) using observations and model simulations. In 2015/2016, the O_3 column was comparably low in early winter, but from February onwards the O_3 column started to increase significantly due to the disturbances of the Arctic stratosphere by sudden stratospheric warmings. In fact, winters with above average stratospheric wave activity have a warm, disturbed vortex, while winters with weak wave driving have a cold, long lasting vortex, with well-known impacts on Arctic March temperatures and O_3 column (Strahan et al. (2013) and references therein). Manney and Lawrence (2016) found from MLS observations that ozone continued to decrease in the vortex at a rate slightly faster than that in 2011 until the beginning of March 2016. However, around mid-March ozone increased for the rest of the winter, so that the ozone values always remained higher than in 2011. This is also seen in the EMAC simulation. Therefore, our model simulations are in agreement with the results by Manney and Lawrence (2016) who showed that in the Arctic winter 2015/2016 the stratosphere appeared to have the greatest potential yet seen for a massive Arctic ozone loss due to record low temperatures, but was disrupted by the final sudden warming in early March. In other words, massive Arctic ozone loss likely would have occurred in the Arctic winter 2015/2016 if the vortex had remained stable and temperatures remained low through into late March.

On the other hand, although ozone loss was not stronger than in 2010/2011, denitrification and dehydration were the strongest observed so far (Manney and Lawrence, 2016). From the EMAC simulation the same result as from the observations is derived. Figure 11 shows the time series of HNO_3 and H_2O for the same four Arctic winters as shown in Fig. 10. At $48\,hPa$ several ppbv lower HNO_3 mixing ratios than in previous cold Arctic winters is found from December to February. Pre-winter HNO_3 mixing ratios were around $11\,ppbv$ and drop to $4\,ppbv$ in mid January. How much lower the H_2O mixing ratios drop due to the dehydration during the Arctic winter 2015/2016 compared to other Arctic winters can be seen in the H_2O time series at $48\,hPa$ (Fig. 11 bottom). In early December, H_2O mixing ratios are as high as $5.8\,ppmv$ and decrease to $5.2\,ppmv$, but decrease for

9

a short period towards the end of January to even lower values (4.7 ppmv). From the end of January the H_2O mixing ratios increase slowly, but still remain lower than the pre-winter values. The H_2O mixing ratios are in addition $\sim$1-1.5 ppmv lower in January and February than in previous cold Arctic winters.

4 Comparison to observations

In this study, we compare the EMAC simulations for the Arctic winter 2015/2016 to Aura/MLS observations. In another study Khosrawi et al. (2017) the EMAC simulations of HNO_3, temperature and PSC volume density were compared for the Arctic winters 2009/2010 and 2010/2011 with satellite observations (Envisat/MIPAS and Aura/MLS). Here, we consider in addition to temperature and HNO_3 other trace gases such as O_3, ClO (section 4.1) as well as H_2O and compare the simulations to Aura/MLS observations. Additionally, the EMAC simulations are compared to remote sensing observations from GLORIA performed during the POLSTRACC measurement campaign (section 4.2). For the comparisons to Aura/MLS the EMAC SORBIT output is used (Jöckel et al., 2010) while for the comparison to GLORIA the EMAC global field output is interpolated to the GLORIA measurement geolocations.

4.1 Comparison to Aura/MLS

Figure 12 shows a comparison of the temperature, HNO_3, and O_3 distribution measured by Aura/MLS with the ones simulated with EMAC at about $50\,hPa$ on 15 January 2016. For temperature as well as for HNO_3 and O_3 the simulations are in general agreement with the Aura/MLS observations. Nevertheless, some differences are found between model simulations and observations. Temperatures as simulated with EMAC (nudged towards ECMWF operational analyses) tend to be slightly higher than measured outside the polar vortex. The trace gas distributions of HNO_3 and O_3 simulated with EMAC show more fine-scale structures which may be related to the higher horizontal resolution ($1.125° \times 1.125° \sim 125\,km \times 125\,km$ or less dependent on latitude) of the EMAC simulation compared to Aura/MLS (measurements every $1.5° \sim 165\,km$ and resolution of 200-500 km along track). Generally, the simulated HNO_3 mixing ratios are slightly lower than the ones measured with Aura/MLS while the simulated O_3 mixing ratios are quite similar to the observed O_3.

The temporal development of ClO, HNO_3 and O_3 averaged over 70-90°N during the Arctic winter 2015/2016 as function of pressure as simulated with EMAC and observed by Aura/MLS is shown in Fig. 13. Here, the EMAC SORBIT output is used (Jöckel et al., 2010) where EMAC is sampled along the sun-synchronous orbit of Aura/MLS. The use of the SORBIT output improves the agreement between observations and simulations of trace gases with a diurnal cycle as e. g. ClO significantly, but has a rather minor impact on the comparison between observations and simulations for other trace gases such s e. g. O_3. Generally, the temporal evolution of the trace gas distributions is realistically reproduced in the EMAC simulation. Nevertheless, there are some differences found between measurement and model simulations. In the observations, increased ClO mixing ratios are already found in December whereas in the model simulation the increase of ClO occurs somewhat later. However, the enhancement of ClO_x (ClO_x=Cl+ClO+HOCl+OClO+2·Cl_2+2·Cl_2O_2) in the EMAC simulation is found at the same time as in the Aura/MLS ClO observation, thus indicating that the later increase in ClO is not necessarily caused by the activation

of chlorine being too late in the model simulation but could also be caused by the partitioning between the active chlorine species. In EMAC the photolyses rates are calculated by the submodel JVAL (Section 2.1). JVAL is part of the standard configuration of EMAC that was also used in the EMAC simulations contributing to the Chemistry-Climate Model Initiative (CCMI, (Jöckel et al., 2016)). An intercomparison of several photolyses schemes has shown that JVAL provides lower photolysis rates

5   at very high solar zenith angles (>90°) for e.g. Cl_2O_2 than other schemes. Thus, the partitioning of chlorine containing species may be shifted for high solar zenith angles and thus could be the cause for the delay in the activation of ClO in the model simulation. However, to entirely rule out the cause for this difference further studies are necessary which are beyond the scope of this study. The ClO mixing ratios are maximum in February in both the observations and model simulations. However, at the maximum higher mixing ratios are found and these extend over a larger vertical range in the EMAC simulation than in

10   Aura/MLS observations.

The temporal evolution of the HNO_3 distribution as a function of pressure shows that the model simulation captures the general features well. In early December HNO_3 mixing ratios are slightly underestimated by EMAC ($\sim$1 ppbv). Gas phase removal of HNO_3 due to uptake in PSCs is more strongly simulated at higher pressure levels (December to January at around 100 hPa) while underestimated at lower pressure levels (January to February at around 50 hPa). PSCs composed of NAT form

15   in EMAC as soon as temperatures drop below T_{NAT}-3 K which often results in a too early formation of NAT particles. Among other things, this has also an impact on the denitrification as was found in another study comparing EMAC simulations for the Arctic winter 2009/2010 and 2010/2011 with Envisat/MIPAS and Aura/MLS observations (Khosrawi et al., 2017). Because NAT is calculated before STS in the model, the NAT formation occurs at the expense of STS since the available HNO_3 is first consumed by the NAT clouds (e.g., Wohltmann et al., 2013). Since in reality STS and NAT clouds are often observed at

20   the same time (e.g., Pitts et al., 2011; Peter and Grooß, 2012), this could be one explanation for the deviations in the HNO_3 distribution.

The temporal evolution of EMAC O_3 (Fig. 13 bottom panel) is quite similar to that observed by Aura/MLS, especially in the lower stratosphere. In the upper stratosphere more O_3 is brought down leading to higher O_3 in the EMAC simulation above 20 hPa in March compared to Aura/MLS.

25   Figure 14 shows the time series of HNO_3 and O_3 at 50 hPa for Aura/MLS and the EMAC T42 and T106 simulation. In the EMAC simulation the HNO_3 is slightly underestimated in the beginning of December (by about 1 ppbv). Larger differences at 50 hPa are found in the time period of denitrification (end of December to end of January). At this time, the EMAC simulations underestimate denitrification at 50 hPa by about 2-3 ppbv. The simulated O_3 is in good agreement with Aura/MLS measurements during December and January. From February onwards the simulated O_3 is up to 0.25 ppmv higher than the

30   observed O_3. For both species the T106L90 simulation agrees slightly better with the Aura/MLS observations.

4.2   Comparison to GLORIA

The EMAC simulations were performed in support of the POLSTRACC campaign. This allows as to evaluate the model performance in the lower stratosphere by comparison to high resolved measurements performed onboard HALO. Here, we show a comparison of EMAC HNO_3 and O_3 to the remote sensing instrument GLORIA. The comparison shown here is

for the POLSTRACC flight 21 on 18 March 2016. EMAC output has been taken along the times and location of GLORIA measurements (Fig. 15). The GLORIA measurements in chemistry mode of flight 21 used in this comparison were performed over Scandinavia. By mid-March the polar vortex had been displaced off the pole and split. The colder offspring vortex was centered over Northern Russia and during flight 21 air masses at the border of this offspring vortex have been probed.

5   EMAC HNO_3 and O_3 compares generally well to GLORIA in terms of the distribution and mixing ratios. However, at 12-14 km, the area where the polar vortex has been probed, O_3 mixing ratios from EMAC are slightly lower than the ones observed by GLORIA. The same holds for HNO_3, but differences between EMAC and GLORIA are larger. The underestimation of polar vortex O_3 in the EMAC simulation could be either caused by a too weak downward transport or a too strong ozone destruction in the model. The former reason, however, is more likely, since a well known feature in EMAC is that the downward transport

10   is underestimated in the lower parts of the polar vortices (Brühl et al., 2007), despite the model vorticity and divergence fields being nudged towards ECMWF analyses. Further, ozone loss in EMAC is rather underestimated than overestimated as was found in the evaluation study by Khosrawi et al. (2009).

Another difference between EMAC and GLORIA is that less fine-scale structure is simulated with EMAC than observed by GLORIA, which is probably due to the rather coarse horizontal resolution of EMAC (T106 corresponding to $1.125° \times$

15   $1.125°$) compared to GLORIA. Nevertheless, these results show that EMAC simulations can be used for comparisons to aircraft measurements. In the future simulations with EMAC with an even higher horizontal resolution (T255) are anticipated which are expected to result in even better agreement with observations derived onboard aircraft. However, it should be kept in mind that a good agreement between model simulations and observations can only be obtained if the model simulations are nudged towards meteorological analyses. It can be expected that comparison with free running model simulations would show

20   larger differences. Further, the results are also limited by the accuracy of the meteorological analyses, e.g. resolving small-scale temperature fluctuations and mountain waves will still be problematic even when a T255 resolution is used.

5   Conclusions

In this study, an overview of the chemistry and dynamics of the Arctic winter 2015/2016 as simulated with EMAC was given. The EMAC simulations were performed with a T106L90 resolution and nudged toward ECMWF operational analyses.

25   Chemical-dynamical processes such as denitrification, dehydration and ozone loss were investigated and comparisons to satellite observations by the Aura/MLS as well as to airborne measurements with GLORIA performed onboard of HALO were shown.

From the EMAC simulation we derive a maximum polar stratospheric O_3 loss of $\sim$2 ppmv or 117 DU in terms of column in mid March (averaged over 70-90°N). Note that we did not use equivalent latitudes here since separation between chemical

30   and dynamical processes is achieved via the passive O_3 tracer. On equivalent latitudes the same amount of ozone loss in terms of mixing ratio is derived while in terms of column loss ozone loss is 10% less (103 DU). The stratosphere was denitrified by about 4-8 ppbv HNO_3 and dehydrated by about 0.6-1 ppmv H_2O in mid to end of February. In agreement with the analyses of Aura/MLS observations by Manney and Lawrence (2016) we find that ozone loss was quite strong in 2015/2016, but not

as strong as in 2010/2011. Denitrification and dehydration on the other hand were so far the strongest observed in the Arctic stratosphere.

Comparison of trace gas distributions of HNO_3, ClO and O_3 shows that the EMAC simulations nudged toward ECMWF operational analyses generally reproduce well the Aura/MLS observations during the Arctic winter 2015/2016. However, there are some differences between the EMAC simulations and observations which need sensitivity studies in the future to improve the agreement between the model simulations and observations. In the EMAC simulation HNO_3 is slightly underestimated (by about $1\,\mathrm{ppbv}$). Larger differences are found in the area of denitrification which could be related to the partitioning between STS and NAT in the model. The observed increase in ClO at the beginning of the winter is simulated later with EMAC. Since the enhancement in modelled ClO_x is found roughly at the same time as the observed increase in ClO, the disparity in the behaviour of modelled and measured ClO may arise from chlorine activation being delayed in the model due to inaccuracies in the partitioning between chlorine species at high solar zenith angles.

The comparison to GLORIA measurements shows that EMAC simulations nudged toward ECMWF operational analyses can reproduce the observations. Further, this comparison shows that, though EMAC is a climate model, EMAC simulations can be applied in support of aircraft campaigns and that these simulations provide a valuable data set not only for flight analyses but also for measurement - model intercomparisons.

References

Atkinson, R., Baulch, D. L., Cox, R. A., Crowley, J. N., Hampson, R. F., Hynes, R. G., Jenkin, M. E., Rossi, M. J., and Troe, J.: Evaluated kinetic and photochemical data for atmospheric chemistry: Volume III gas phase reactions of inorganic halogens, Atmos. Chem. Phys., pp. 981–1191, doi:10.5194/acp–7–981–2007, 2007.

5 Brühl, C., Steil, B., Stiller, G., Funke, B., and Jöckel, P.: Nitrogen compounds and ozone in the stratosphere: comparison of MIPAS satellite data with the chemistry climate model ECHAM5/MESSy1, Atmos. Chem. Phys., 7, 5585–5598, 2007.

Carslaw, K. S., Luo, B. P., Clegg, S. L., Peter, T., Brimblecombe, P., and Crutzen, P. J.: Stratospheric aerosol growth and HNO_3 gas phase depletion from coupled HNO_3 and water uptake by liquid particles, Geophys. Res. Lett., 21, 2479–2482, 1994.

Carslaw, K. S., Clegg, S. L., and Brimblecombe, P.: A thermodynamic model of the system HCl-HNO_3-H_2SO_4-H_2O, including solubilities
10 of HBr, from 328 K to < 200 K, J. Phys. Chem., 99, 11 557–11 574, 1995.

Carslaw, K. S., Kettleborough, J., Northway, M. J., Davies, S., Gao, R.-S., Fahey, D. W., Baumgardner, D. G., Chipperfield, M. P., and Kleinböhl, A.: A vortex-wide simulation of the growth and sedimentation of large nitric acid hydrate particles, J. Geophys. Res., 107, 8300, doi:10.1029/2011JD000 467, 2002.

Crutzen, P. J. and Arnold, F.: Nitric acid cloud formation in the cold Antarctic stratosphere: A major cause for the springtime 'ozone hole',
15 Nature, 342, 651–655, 1986.

Dee, D. P., Uppala, S. M., Simmons, A. J., Berrisford, P., Poli, P., Kobayashi, S., Andrae, U., Balmaseda, M. A., Balsamo, G., Bauer, P., Bechtold, P., Beljaars, A. C. M., van de Berg, L., Bidlot, J., Bormann, N., Delsol, C., Dragani, R., Fuentes, M., Geer, A. J., Haimberger, L., Healy, S. B., Hersbach, H., Hólm, E. V., Isaksen, L., Kållberg, P., Köhler, M., Matricardi, M., McNally, A. P., Monge-Sanz, B. M., Morcrette, J.-J., Park, B.-K., Peubey, C., deRosnay, P., Tavolato, C., Thépaut, J.-N., and Vitart, F.: The ERA-Interim reanalysis: configuration
20 and performance of the data assimilation system, Q. J. R. Meteorol. Soc., 137, 553–597, 2011.

Dörnbrack, A., Gisinger, S., Pitts, M. C., Poole, L. R., and Maturilli, M.: Multilevel cloud structures over Svalbard, Mon. Weather. Rev., pp. 1149–1159, doi:10.1175/mwr–d–16–0214.1, 2017.

Engel, A., Schiller, C., Schmidt, U., Borchers, R., Ovarlez, H., and Ovarlez, J.: The total hydrogen budget in the Arctic winter stratosphere during the European Arctic Stratospheric Ozone Experiment, J. Geophys. Res., 101, 14 495–14 503, 1996.

25 Fahey, D. W., Kelly, K. K., Ferry, G. V., Poole, L. R., Wilson, J. C., Murphy, D. M., Loewenstein, M., and Chan, K. R.: In situ measurements of total reactive nitrogen, total water, and aerosol in a polar stratospheric cloud in the Antarctic, J. Geophys. Res., 94, 11 299–11 315, 1989.

Fahey, D. W., Kelly, K. K., Kawa, S. R., Tuck, A. F., Loewenstein, M., Chan, K. R., and Heid, L. E.: Observations of denitrification and dehydration in the winter polar stratosphere, Nature, 344, 321–324, 1990.

30 Fahey, D. W., Gao, R. S., Carslaw, K. S., Kettleborough, J., Popp, P. J., Northway, M. J., Holecek, J. C., Ciciora, S. C., McLaughlin, R. J., Thompson, T. L., Winkler, R. H., Baumgardner, D. G., Gandrud, B., Wennberg, P. O., Dhaniyala, S., McKinley, K., Peter, T., Salawitch, R. J., Bui, T. P., Elkins, J. W., Webster, C. R., Atlas, E. L., Jost, H., Wilson, J. C., Herman, R. L., Kleinböhl, A., and von König, M.: The detection of large HNO_3-containing particles in the winter Arctic stratosphere, Science, 291, 1026–1031, 2001.

Friedl-Vallon, F., Gulde, T., Hase, F., Kleinert, A., Kulessa, T., Maucher, G., Neubert, T., Olschewski, F., Piesch, C., Preusse, P., Rongen, H.,
35 Sartorius, C., Schneider, H., Schönfeld, A., Tan, V., Bayer, N., Blank, J., Dapp, R., Ebersoldt, A., Fischer, H., Graf, F., Guggenmoser, T., Höpfner, M., Kaufmann, M., Kretschmer, E., Latzko, T., Nordmeyer, H., Oelhaf, H., Orphal, J., Riese, M., Schardt, G., Schillings, J., Sha,

14

M. K., Suminska-Ebersoldt, O., and Ungermann, J.: Instrument concept of the imaging Fourier transform spectrometer GLORIA, Atmos. Meas. Tech., 7, 3565–3577, doi:10.5194/amt–7–3565–2014, 2014.

Froidevaux, L., Jiang, Y. B., Lambert, A., Livesey, N. J., Read, W. G., Waters, J. W., Browell, E. V., Hair, J. W., Avery, M. A., McGee, T. J., Twigg, L. W., Sumnicht, G. K., Jucks, K. W., Margitan, J. J., Sen, B., Stachnik, R. A., Toon, G. C., Bernath, P. F., Boone, C. D., Walker, K. A., Filipiak, M. J., Harwood, R. S., Fuller, R. A., Manney, G. L., Schwartz, M. J., Daffer, W. H., Drouin, B. J., Cofield, R. E., Cuddy, D. T., Jarnot, R. F., Knosp, B. W., Perun, V. S., Snyder, W. V., Stek, P. C., Thurstans, R. P., and Wagner, P. A.: Validation of Aura Microwave Limb Sounder stratospheric ozone measurements, J. Geophys. Res., 113, D15S20, doi:10.1029/2007JD008 771, 2008.

Fueglistaler, S., Luo, B. P., Voigt, C., Carslaw, K. S., and Peter, T.: NAT-rock formation by mother clouds: a microphysical model study, Atmos. Chem. Phys., 2, 93–98, doi:10.5194/acp–2–93–2002, 2002.

Hanson, D. R. and Mauersberger, K.: Laboratory studies of the nitric acid trihydrate: Implications for the south polar stratosphere, Geophys. Res. Lett., 15, 855–858, 1988.

Hommel, R., Eichmann, K.-U., Bramstedt, J. A. K., Weber, M., von Savigny, C., Richter, A., Rozanov, A., Khosrawi, F., Bauer, R., and Burrows, J. P.: Chemical ozone loss and ozone mini-hole event during the Arctic winter 2010/2011 as observed by SCIAMACHY and GOME-2, Atmos. Chem. Phys., 14, 3247–3276, 2014.

Hoyle, C. R., Engel, I., Luo, B. P., Pitts, M. C., Poole, L. R., Grooß, J.-U., and Peter, T.: Heterogeneous formation of polar stratospheric clouds - Part 1: Nucleation of nitric acid trihydrate (NAT), Atmos. Chem. Phys., 14, 9577–9595, 2013.

Jiang, Y. B., Froidevaux, L., Lambert, A., Livesey, N. J., Read, W. G., Waters, J. W., Bojkov, B., Leblanc, T., McDermid, I. S., Godin-Beekmann, S., Filipiak, M. J., Harwood, R. S., Fuller, R. A., Daffer, W. H., Drouin, B. J., Cofield, R. E., Cuddy, D. T., Jarnot, R. F., Knosp, B. W., Perun, V. S., Schwartz, M. J., Snyder, W. V., Stek, P. C., Thurstans, R. P., Wagner, P. A., Allaart, M., Andersen, S. B., Bodeker, G., Calpini, B., Claude, H., Coetzee, G., Davies, J., De Backer, H., Dier, H., Fujiwara, M., Johnson, B., Kelder, H., Leme, N. P., Konig-Langlo, G., Kyro, E., Laneve, G., Fook, L. S., Merrill, J., Morris, G., Newchurch, M., Oltmans, S., Parrondos, M. C., Posny, F., Schmidlin, F., Skrivankova, P., Stubi, R., Thompson, D. T. A., Thouret, V., Viatte, P., Vömel, H., von Der Gathen, P., Yela, M., and Zablocki, G.: Validation of Aura Microwave Limb Sounder Ozone by ozonesonde and lidar measurements, J. Geophys. Res., 112, D24S34, doi:10.1029/2007JD008 776, 2007.

Jöckel, P., Kerkweg, A., Pozzer, A., Sander, R., Tost, H., Riede, H., Baumgaertner, A., Gromov, S., and Kern, B.: Development cycle 2 of the Modular Earth Submodel System (MESSy2), Geosci. Model Dev., 3, 717–752, doi:10.5194/gmd–3–717–2010, 2010.

Jöckel, P., Tost, H., Pozzer, A., Kunze, M., Kirner, O., Brenninkmeijer, C. A. M., Brinkop, S., Cai, D. S., Dyroff, C., Eckstein, J., Frank, F., Garny, H., Gottschaldt, K.-D., Graf, P., Grewe, V., Kerkweg, A., Kern, B., Matthes, S., Mertens, M., Meul, S., Neumaier, M., Nützel, M., Oberländer-Hayn, S., Ruhnke, R., Runde, T., Sander, R., Scharffe, D., and Zahn, A.: Earth System Chemistry Integrated Modelling (ESCiMo) with the Modular Earth Submodel (MESSy, version 2.51), Geosci. Model Dev., 9, 1153–1200, doi:10.5194/gmdd–9–1153–201, 2016.

Kelly, K. K., Tuck, A. F., Murphy, D. M., Proffitt, M. H., Fahey, D. W., Jones, R. L., McKenna, D. S., Loewenstein, M., Podolske, J. R., Strahan, S. E., Ferry and K. R. Chan and J. F. Vedder, G. V., Gregory, G. L., Hypes, W. D., McCormick, M. P., Browell, E. V., and Heidt, L. E.: Dehydration in the lower Antarctic stratosphere during late winter and early spring, 1987, J. Geophys. Res., 94, 11 317–11 357, 1989.

Khaykin, S. M., Engel, I., Vömel, H., Formanyuk, I. M., Kivi, R., Korshunov, L. I., Krämer, M., Lykov, A. D., Meier, S., Naebert, T., Pitts, M. C., Santee, M. L., Spelten, N., Wienhold, F. G., Yushkov, V. A., and Peter, T.: Arctic stratospheric dehydration – Part 1: Unprecedented observation of vertical redistribution of water, Atmos. Chem. Phys., 13, 11 503–11 517, doi:10.5194/acp–13–11 503–2013, 2013.

Khosrawi, F., Müller, R., Proffitt, M. H., Ruhnke, R., Kirner, O., Grooss, J.-U., Murtagh, D. P., and Nakajima, H.: Evaluation of CLaMS, KASIMA and ECHAM5/MESSy1 simulations in the Northern Hemisphere lower stratosphere using observations of Odin/SMR and ILAS/ILAS-II, Atm. Chem. Phys., 9, 5759–5783, 2009.

Khosrawi, F., Kirner, O., Stiller, G., Höpfner, M., Santee, M. L., Kellmann, S., and Braesicke, P.: Comparison of ECHAM5/MESSy Atmospheric Chemistry (EMAC) Simulations of the Arctic winter 2009/2010 and 2010/2011 with Envisat/MIPAS and Aura/MLS Observations, Atmos. Chem. Phys., 17, to be submitted, 2017.

Kirner, O., Ruhnke, R., Buchholz-Dietsch, J., Jöckel, P., Brühl, C., and Steil, B.: Simulation of polar stratospheric clouds in the chemistry-climate model EMAC via the submodel PSC, Geosci. Model Dev., 4, 169–182, doi:10.5194/gmd–4–169–2011, 2011.

Kleinert, A., Friedl-Vallon, F., Guggenmoser, T., Höpfner, M., Neubert, T., Ribalda, R., Sha, M. K., Ungermann, J., Blank, J., Ebersoldt, A., Kretschmer, E., Latzko, T., Oelhaf, H., Olschewski, F., and Preusse, P.: Level 0 to 1 processing of the imaging Fourier transform spectrometer GLORIA: generation of radiometrically and spectrally calibrated spectra, Atmos. Meas. Tech., 7, 4167–4184, doi:10.5194/amt–7–4167–2014, 2014.

Kondo, Y., Irie, H., Koike, M., and Bodecker, G.: Denitrification and nitrification in the Arctic stratosphere during the winter of 1996-1997, Geophys. Res. Lett., 27, 337–340, 2000.

Koop, T., Biermann, U. M., Raber, W., Luo, B. P., Crutzen, P. J., and Peter, T.: Do stratospheric aerosol droplets freeze above the ice frost point?, Geophys. Res. Lett., 22, 917–920, 1995.

LeTexier, H., Solomon, S., and Garcia, R. R.: The role of molecular hydrogen and methane oxidation in the water vapour budget of the stratosphere, Q. J. R. Meteorol. Soc., 114, 281 – 295, 1988.

Livesey, N. J., Filipiak, M. J., Froidevaux, L., Read, W. G., Lambert, A., Santee, M. L., Jiang, J. H., Pumphrey, H. C., Waters, J. W., Cofield, R. E., Cuddy, D. T., Daffer, W. H., Drouin, B. J., Fuller, R. A., Jarnot, R. F., Jiang, Y. B., Knosp, B. W., Li, Q. B., Perun, V. S., Schwartz, M. J., Snyder, W. V., Stek, P. C., Thurstans, R. P., Wagner, P. A., Avery, M., Browell, E. V., Cammas, J.-P., Christensen, L. E., Diskin, G. S., Gao, R.-S., Jost, H.-J., Loewenstein, M., Lopez, J. D., Nedelec, P., Osterman, G. B., Sachse, G. W., and Webster, C. R.: Validation of Aura Microwave Limb Sounder O_3 and CO observations in the upper troposphere and lower stratosphere, J. Geophys. Res., 113, D15S02, doi:10.1029/2007JD008 805, 2008.

Livesey, N. J., Read, W. G., Froidevaux, L., Lambert, A., Manney, G. L., Pumphrey, H. C., Santee, M. L., Schwartz, M. J., Wang, S., Cofield, R. E., Cuddy, D. T., Fuller, R. A., Jarnot, R. F., Jiang, J. H., Knosp, B. W., Stek, P. C., Wagner, P. A., and Wu, D. L.: Aura Microwave Limb Sounder (MLS) Version 3.3 and 3.4 Level 2 data quality and description document, Tech. Rep. JPL D-33509, available from: http://mls.jpl.nasa.gov/, 2013.

Livesey, N. J., Santee, M. L., and Manney, G. L.: A Match-based approach to the estimation of polar stratospheric ozone loss using Aura Microwave Limb Sounder observations, 2015.

Livesey, N. J., Read, W. G., Wagner, P. A., Froidevaux, L., Lambert, A., Manney, G. L., Millán Valle, L. F., Pumphrey, H. C., Santee, M. L., Schwartz, M. J., Wang, S., Fuller, R. A., Jarnot, R. F., Knosp, B. W., and Martinez, E.: Aura Microwave Limb Sounder (MLS) Version 4.2x Level 2 data quality and description document, Tech. Rep. JPL D-33509 Rev. C, available from: http://mls.jpl.nasa.gov/, 2017.

Lowe, D. and MacKenzie, R.: Review: Polar stratospheric cloud microphysics and chemistry, J. Atm. Sol. Terr. Phys., 70, 13–40, 2008.

Manney, G. L. and Lawrence, Z. D.: The major stratospheric final warming in 2016: dispersal of vortex air and termination of Arctic chemical ozone loss, Atmos. Chem. Phys., 16, 15 371–15 396, doi:10.5194/acp–16–15 371–2016, 2016.

Manney, G. L., Santee, M. L., Froidevaux, L., Hoppel, K., Livesey, N. J., and Waters, J. W.: EOS MLS observations of ozone loss in the 2004-2005 Arctic winter, Geophys. Res. Lett., 33, L04 802, doi:10.1029/2005GL024 494, 2006.

Manney, G. L., Santee, M. L., Rex, M., Livesey, N. L., Pitts, M. C., Veefkind, P., Nash, E. R., Woltmann, I., Lehmann, R., Froidevaux, L., Poole, L. R., Schoeberl, M. R., Haffner, D. P., Davies, J., Dorokhov, V., Gernandt, H., Johnson, B., Kivi, R., Kyrö, E., Larsen, N., Levelt, P. F., Makshtas, A., McElroy, C. T., Nakajima, H., Concepcion Parrondo, M., Tarasick, D. W., von der Gathen, P., Walker, K. A., and Zinoviev, N. S.: Unprecedented Arctic ozone loss in 2011, Nature, 478, doi:10.1038/nature10 556, 469–475, 2011.

5   Marti, J. and Mauersberger, K.: A survey and new measurements of ice vapor pressure temperatures between 170 and 250 K, Geophys. Res. Lett., 20, 363–366, 1993.

Matthias, V., Dörnbrack, A., and Stober, G.: The extraordinarily strong and cold polar vortex on the early northern winter 2015/16, Geophys. Res. Lett., 43, 12 287–12 294, doi:10.1002/2016GL071 676, 2016.

Nedoluha, G. E., Bevilacqua, R. M., Hoppel, K. W., Daehler, M., Shettle, E. P., Homstein, J. H., Fromm, M. D., Lumpe, J. D., and Rosenfield, J. E.: POAM III measurements of dehydration in the Antarctic lower stratosphere, Geophys. Res. Lett., 27, 1683–1686, 2000.

Pan, L. L., Randel, W. J., Nakajima, H., Massie, S. T., Kanzawa, H., Sasano, Y., Sugita, T., Hayashida, S., and Oshchepkov, S.: Satellite observation of dehydration in the Arctic polar stratosphere, Geophys. Res. Lett., 29, 1184, doi.10.1029/2001GL014 147, 2002.

Peter, T.: Microphysics and heterogeneous chemistry of polar stratospheric clouds, Annu. Rev. Phys. Chem., 48, 785–822, 1997.

Peter, T. and Grooß, J.-U.: Chapter 4: Polar stratospheric clouds and sulfate aerosol particles: Microphysics, denitrification and heterogeneous chemistry, in: Stratospheric Ozone Depletion and Climate, edited by Müller, R., pp. 108–144, RSC Publishing, 2012.

Pitts, M. C., Poole, L. R., Dörnbrack, A., and Thomason, L. W.: The 2009-2010 Arctic polar stratospheric cloud season: a CALIPSO perspective, Atmos. Chem. Phys, pp. 2161–2177, doi:10.5194/acp–11–2161–2011, 2011.

Rex, M., Harris, N. R. P., von der Gathen, P., Lehmann, R., Braathen, G. O., Reimer, E., Beck, A., Chipperfield, M., Alfier, R., Allaart, M., O'Connor, F., Dier, H., Dorokhov, V., Fast, H., Gil, M., Kyrö, E., Litynska, Z., Mikkelsen, I. S., Molyneux, M., Nakane, H., Notholt, J., Rummukainen, M., Viatte, P., and Wenger, J.: Prolonged stratospheric ozone loss in the 1995/96 Arctic winter, Nature, 389, 835–838, 1997.

Riese, M., Oelhaf, H., Preusse, P., Blank, J., Ern, M., Friedl-Vallon, F., Fischer, H., Guggenmoser, T., Höpfner, M., Hoor, P., Kaufmann, M., Orphal, J., Plöger, F., Spang, R., Suminska-Ebersoldt, O., Ungermann, J., Vogel, B., and Woiwode, W.: Gimballed Limb Observer for Radiance Imaging of the Atmosphere (GLORIA) scientific objectives, Atmos. Meas. Tech., 7, 1915–1928, doi:10.5194/amt–7–1915–2014, 2014.

Rinsland, C. P., Gunson, M. R., Salawitch, R. J., Newchurch, M. J., Zander, R., Abbas, M. M., Abrams, M. C., Manney, G. L., Michelsen, H. A., Chang, A. Y., and Goldman, A.: ATMOS measurements of H_2O+2CH_4 and total reactive nitrogen in the November 1994 Antarctic stratosphere: Dehydration and denitrification in the vortex, Geophys. Res. Lett., 23, 2397–2400, 1996.

Roeckner, E., Brokopf, R., Esch, M., Giorgetta, M., Hagemann, S., Koernblueh, L., Manzini, E., Schlese, U., and Schulzweida, U.: Sensitivity of simulated climate to horizontal and vertical resolution in the ECHAM5 atmosphere model, J. Climate, 19, 3771–3791, 2006.

Salawitch, R., Wofsy, S., Gottlieb, E., Lait, L., Newman, P., Schoeberl, M., Loewenstein, M., Podolske, J., Strahan, S., Proffitt, M., Webster, C., May, R., Fahey, D., Baumgardner, D., Dye, J., Wilson, J., Kelly, K., Elkins, J., Chan, K., and Anderson, J.: Chemical loss of ozone in the Arctic polar vortex in the winter of 1991-1992, Science, 261, 1146–1154, 1993.

Sander, R., Baumgaertner, A., Gromov, S., Harder, H., Jöckel, P., Kerkweg, A., Kubistin, D., Regelin, E., Riede, H., Sandu, A., Tarborrelli, D., Tost, H., and Xie, Z.-Q.: The atmospheric chemistry box model CABBA/MECCA-3.0, Geosci. Model Dev., 4, 373–380, doi:10.5194/gmd–4–373–2011, 2011a.

Sander, R., Jöckel, P., Kirner, O., Kunert, A. T., Landgraf, J., and Pozzer, A.: The photolysis module JVAL-14, compatible with the MESSy standard, and the JVal Pre-Pocessor (JVPP), Geosci. Model Dev., 7, 2653–2662, doi:10.5194/gmd–7–2653–2014, 2014.

Sander, S. P., Abbatt, J., Barker, J. R., Burkholder, J. B., Friedl, R. R., Golden, D. M., Huie, R. E., Kolb, C. E., Kurylo, M. J., Moortgat, G. K., Orkin, V. L., and Wine, P. H.: Chemical Kinetics and Photochemical Data for Use in Atmospheric Studies, Tech. rep., Evaluation No. 17, JPL Publication 10-6, Jet Propulsion Laboratory, Pasadena, 2011b.

Santee, M. L., Manney, G. L., Livesey, N. J., Waters, and W., J.: UARS Microwave Limb Sounder observations of denitrification and ozone loss in the 2000 Arctic late winter, Geophysical Research Letters, 27, 3213–3216, 10.1029/2000GL011 738, 2000.

Santee, M. L., Lambert, A., Read, W. G., Livesey, N. J., Cofield, R. E., Cuddy, D. T., Daffer, W. H., Drouin, B. J., Froidevaux, L., Fuller, R. A., Jarnot, R. F., Knosp, B. W., Manney, G. L., Perun, V. S., Snyder, W. V., Stek, P. C., Thurstans, R. P., Wagner, P. A., Waters, J. W., Muscari, G., de Zafra, R. L., Dibb, J. E., Fahey, D. W., Popp, P. J., Marcy, T. P., Jucks, K. W., Toon, G. C., Stachnik, R. A., Bernath, P. F., Boone, C. D., Walker, K. A., Urban, J., and Murtagh, D.: Validation of the Aura Microwave Limb Sounder HNO$_3$ measurements, J. Geophys. Res., 112, D24S40, doi:10.1029/2007JD008 721, 2007.

Santee, M. L., Lambert, A., Read, W. G., Livesey, N. J., Manney, G. L., Cofield, R. E., Cuddy, D. T., Daffer, W. H., Drouin, B. J., Froidevaux, L., Fuller, R. A., Jarnot, R. F., Knosp, B. W., Perun, V. S., Snyder, W. V., Stek, P. C., Thurstans, R. P., Wagner, P. A., Waters, J. W., Connor, B., Urban, J., Murtagh, D., Ricaud, P., Barret, B., Kleinböhl, A., Kuttippurath, J., Küllmann, H., von Hobe, M., Toon, G. C., and Stachnik, R. A.: Validation of the Aura Microwave Limb Sounder ClO measurements, J. Geophys. Res., 113, 5S22, doi:10.1029/2007JD008 762, 2008.

Schiller, C., Engel, A., Schmidt, U., R. Borchers, and Ovarlez, J.: The partitioning of hydrogen species in the Arctic winter stratosphere: implications on microphysical parameters, J. Geophys. Res., 101, 14 489–14 493, 1996.

Schiller, C., Bauer, R., Cairo, F., Deshler, T., Dörnbrack, A., Elkins, J., Engel, A., Flentje, H., Larsen, N., Levin, I., Müller, M., Oltmans, S., Ovarlez, H., Ovarlez, J., Schreiner, J., Stroh, F., Voigt, C., and Vömel, H.: Dehydration in the Arctic stratosphere during the SOLVE/THESEO-2000 campaigns, J. Geophys. Res., 107, 8293, doi:10.1029/2001JD000 463, 2002.

Sinnhuber, B.-M., Stiller, G., Ruhnke, R., von Clarmann, T., and Kellmann, S.: Arctic winter 2010/2011 at the brink of an ozone hole, Geophys. Res. Lett., 38, L24 814, doi:10.1029/2011GL049 784, 2011.

Solomon, S.: Stratospheric ozone depletion: A review of concepts and history, Rev. of Geophys., 37, 275–316, 1999.

Solomon, S., Garcia, R. R., Rowland, F. S., and Wuebbles, D. J.: On the depletion of Antarctic ozone, Nature, 321, 755–758, 1986.

Solomon, S., Haskins, J., Ivy, D., and Min, F.: Fundamental differences between Arctic and Antarctic ozone depletion, PNAS, 111, 6220–6225, 2014.

Strahan, S. E., Douglass, A. R., and Newman, P. A.: The contributions of chemistry and transport to low Arctic ozone in March 2011 derived from Aura MLS observations, J. Geophys. Res., 118, 1563–1576, doi:10.1002/jgrd50 181, 2013.

Tilmes, S., Müller, R., Engel, A., and Russel III, J.: Chemical ozone loss in the Arctic and Antarctic stratosphere between 1992 and 2005, Geophys. Res. Lett., 33, L20 812, doi:10.1029/2006GL026 925, 2006.

van den Broek, M. M. P., Williams, J. E., and Bregman, A.: Implementing growth and sedimentation of NAT particles in a global Eulerian model, Atmos. Chem. Phys., 4, 1869–1883, 2004.

Voigt, C., Dörnbrack, A., Wirth, M., Groß, S. M., Baumann, R., Ehard, B., Pitts, M. C., Poole, L. R., Sinnhuber, B.-M., and Oelhaf, H.: Widespread persistent polar stratospheric ice clouds in the Arctic, Atmos. Chem. Phys. Discuss., 16, doi:10.5194/acp–2016–1082, 2016.

Vömel, H., Oltmans, S. J., Hoffmann, D. J., T.Deshler, and Rosen, J. M.: The evolution of the dehydration in the Antarctic stratospheric vortex, J. Geophys. Res., 100, 13,919–13,926, 1995.

Vömel, H., Rummukainen, M., Kivi, R., Karhu, J., Turunen, T., Kyrö, E., Rosen, J., Kjome, N., and Oltmans, S.: Dehydration and sedimentation of ice particles in the Arctic stratospheric vortex, Geophys. Res. Lett., 24, 798–798, 1997.

von Hobe, M., Bekki, S., Borrmann, S., Cairo, F., D'Amato, F., Di Donfrancesco, G., Dörnbrack, A., Ebersoldt, A., Ebert, M., Emde, C., Engel, I., Ern, M., Frey, W., Genco, S., Griessbach, S., Grooß, J.-U., Gulde, T., Günther, G., Hösen, E., Hoffmann, L., Homonnai, V., Hoyle, C. R., Isaksen, I. S. A., Jackson, D. R., Jánosi, I. M., Jones, R. L., Kandler, K., Kalicinsky, C., Keil, A., Khaykin, S. M., Khosrawi, F., Kivi, R., Kuttippurath, J., Laube, J. C., F. Lefévre, Lehmann, R., Ludmann, S., Luo, B. P., Marchand, M., Meyer, J., Mitev, V., Molleker, S., Müller, R., Oelhaf, H., Olschewski, F., Orsolini, Y., Peter, T., Pfeilsticker, K., Piesch, C., Pitts, M. C., Poole, L. R., Pope, F. D., Ravegnani, F., Rex, M., Riese, M., Röckmann, T., Rognerud, B., Roiger, A., Rolf, C., Santee, M. L., Scheibe, M., Schiller, C., Schlager, H., M. Siciliani de Cumis, Sitnikov, N., O. A. Søvde, Spang, R., Spelten, N., Stordal, F., O. Sumińska-Ebersoldt, Ulanovski, A., Ungermann, J., Viciani, S., Volk, C. M., vom Scheidt, M., von der Gathen, P., Walker, K., Wegner, T., Weigel, R., Weinbruch, S., Wetzel, G., Wienhold, F. G., Wohltmann, I., Woiwode, W., Young, I. A. K., Yushkov, V., Zobrist, B., and Stroh, F.: Reconciliation of essential process parameters for an enhanced predictability of Arctic stratospheric ozone loss and its climate interactions (RECONCILE): activities and results, Atmos. Chem. Phys., 13, 9233–9268, 2013.

Waibel, A. E., Peter, T., Carslaw, K. S., Oelhaf, H., Wetzel, G., Crutzen, P. J., Pöschl, U., Tsias, A., Reimer, E., and Fischer, H.: Arctic ozone loss due to denitrification, Science, 283, 2064–2069, 1999.

Waters, J., Froidevaux, L., Harwood, R. S., Jarnot, R. F., Pickett, H. M., Read, W. G., Siegel, P. H., Cofield, R. E., Filipiak, M. J., Flower, D. A., Holden, J. R., Lau, G. K., Livesey, N. J., Manney, G. L., Pumphrey, H. C., Santee, M. L., Wu, D. L., Cuddy, D. T., Lay, R. R., Loo, M. S., Perun, V. S., Schwartz, M. J., Stek, P. C., Thurstans, R. P., Boyles, M. A., Chandra, K. M., Chavez, M. C., Chen, G. S., Chudasama, B. V., Dodge, R., Fuller, R. A., Girard, M. A., Jiang, J. H., Jiang, Y. B., Knosp, B. W., LaBelle, R. C., Lam, J. C., Lee, K. A., Miller, D., Oswald, J. E., Patel, N. C., Pukala, D. M., Quintero, O., Scaff, D. M., Van Snyder, W., Tope, M. C., Wagner, P. A., and Walch, M. J.: The Earth Observing System Microwave Limb Sounder (EOS MLS) on the Aura satellite, IEEE Trans. Geosci. Remote Sens., 44, 1075–1092, 2006.

WMO: Scientific assessment of ozone depletion: 2014, Report No. 55, Geneva, 2010.

Wohltmann, I., Wegner, T., Müller, R., Lehmann, R., Rex, M., Manney, G. L., Santee, M. L., Bernath, P., Sumińska-Ebersoldt, O., Stroh, F., von Hobe, M., Volk, C. M., Hösen, E., Ravegnani, F., Ulanovsky, A., and Yushkov, V.: Uncertainties in modelling heterogeneous chemistry and Arctic ozone depletion in the winter 2009/2010, Atmos. Chem. Phys., 13, 3909–3929, doi:10.5194/acp–2013–3909–2013, 2013.

Woiwode, W., Sumińska-Ebersoldt, O., Oelhaf, H., Höpfner, M., Belyaev, G. V., Ebersoldt, A., Friedl-Vallon, F., Grooß, J.-U., Gulde, T., Kaufmann, M., Kleinert, A., Krämer, M., Kretschmer, E., Kulessa, T., Maucher, G., Neubert, T., Piesch, C., Preusse, P., Riese, M., Rongen, H., Sartorius, C., Schardt, G., Schönfeld, A., Schuettemeyer, D., Sha, M. K., Stroh, F., Ungermann, J., Volk, C. M., and Orphal, J.: Validation of first chemistry mode retrieval results from the new limb-imaging FTS GLORIA with correlative MIPAS-STR observations, Atmos. Meas. Tech., 8, 81–95, doi:10.5194/amt–8–81–2015, 2015.
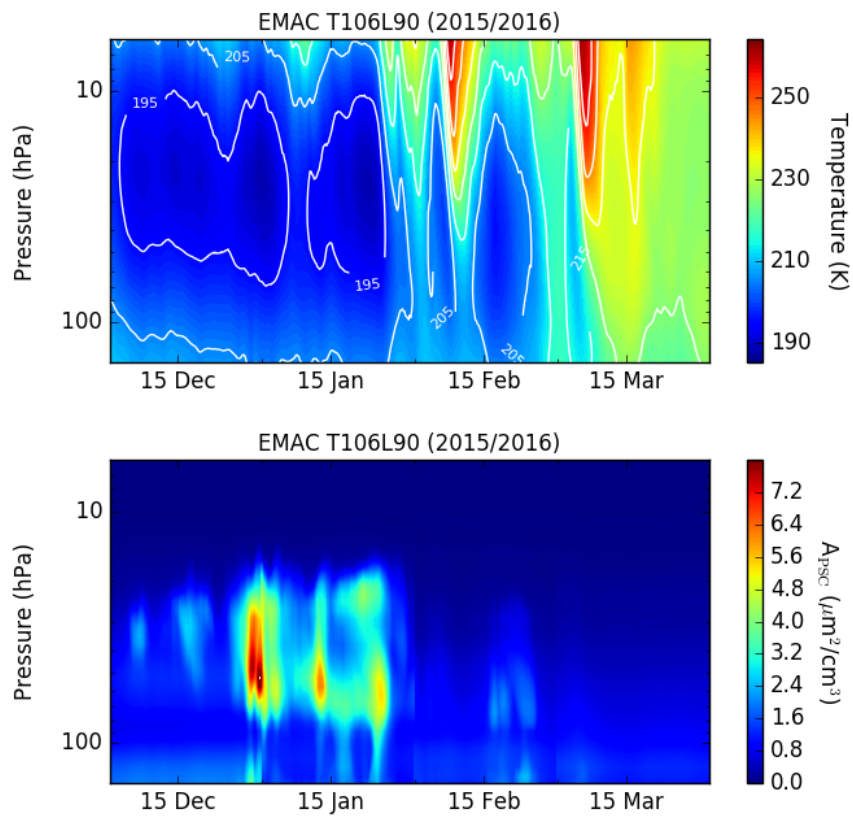
Figure 1. Temporal evolution of temperature and surface area density of PSC particles (liquid + solid) at northern high latitudes (70-90°N) as function of pressure during the Arctic winter 2015/2016 as simulated with EMAC T106L90.
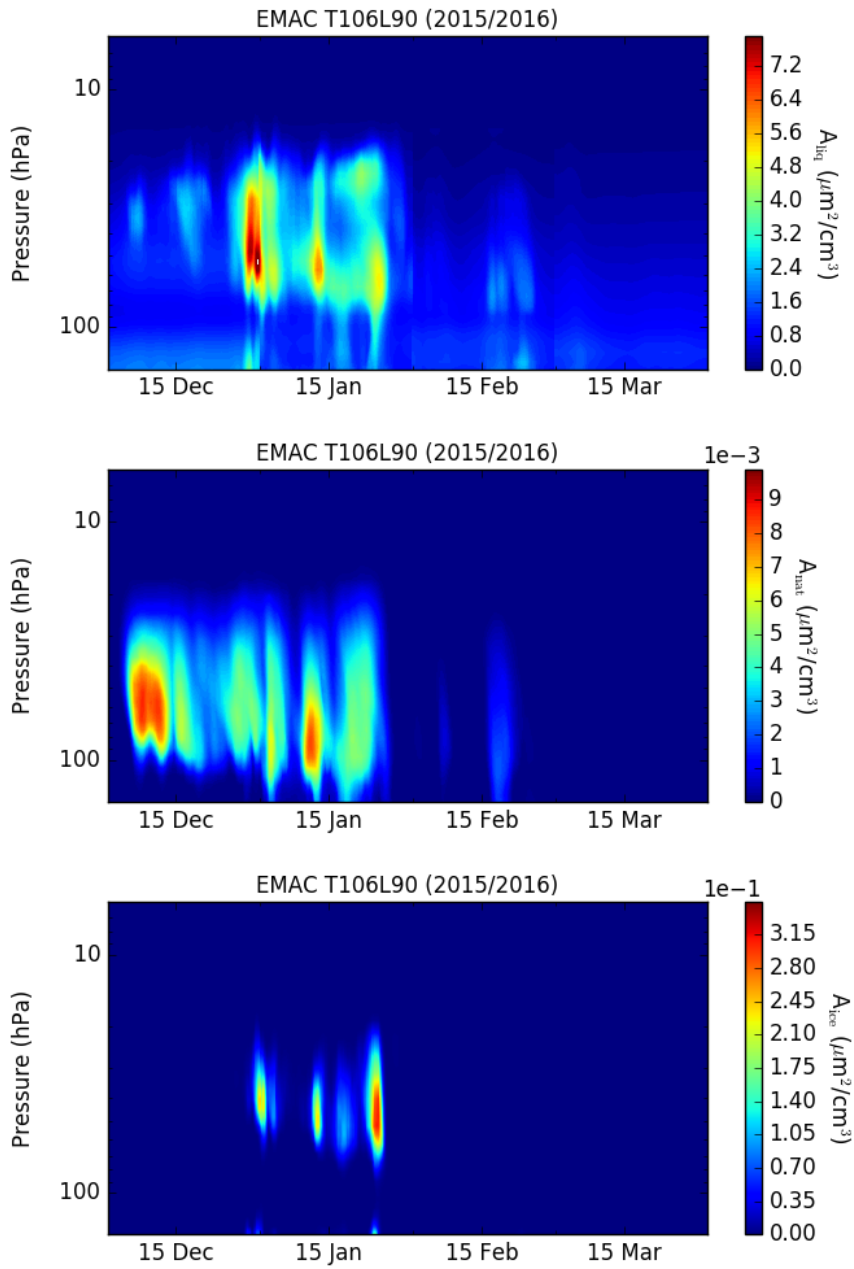
Figure 2. Temporal evolution of surface area density of STS (top), NAT (middle) and ice (bottom) particles at northern high latitudes (70-90°N) as function of pressure during the Arctic winter 2015/2016 as simulated with EMAC T106L90. Note the differences in the color bar for A_{liq} (µm^2/cm^3), A_{NAT} (10^{-3} µm^2/cm^3) and A_{ice} (10^{-1} µm^2/cm^3).

EMAC T106L90 HNO$_3$ at 52 hPa
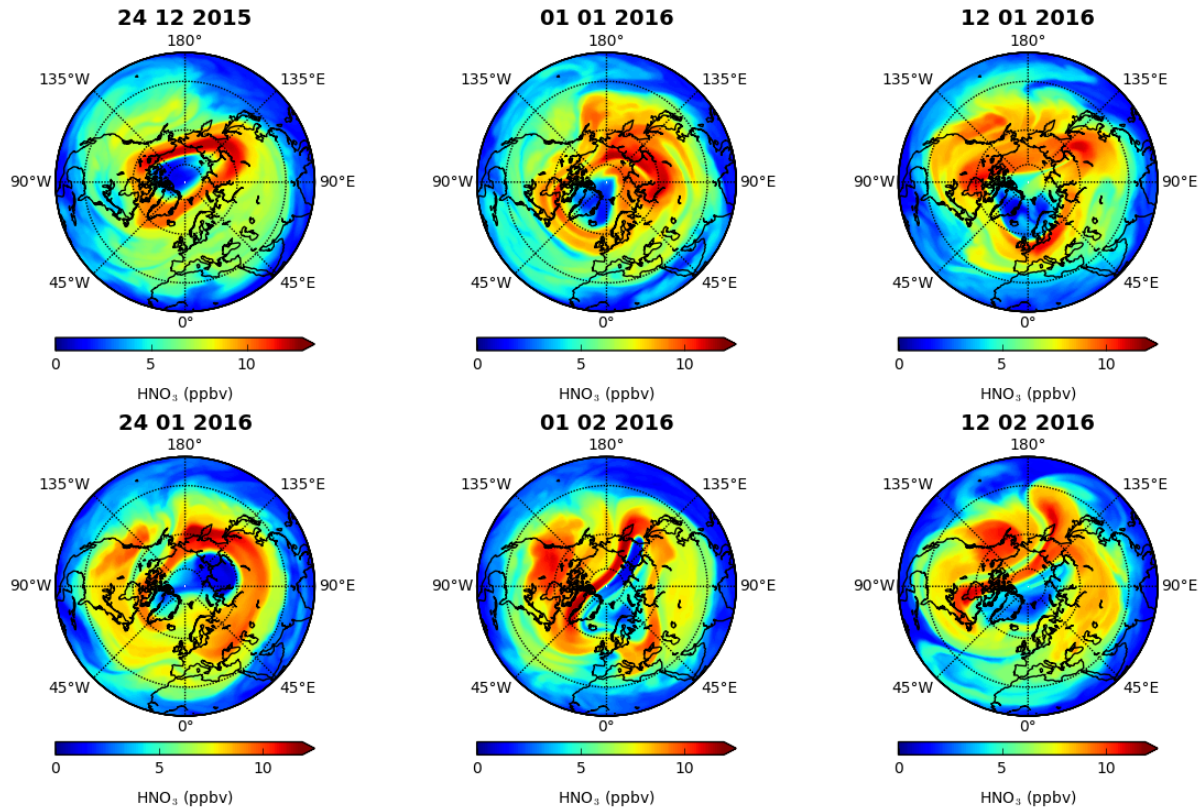
Figure 3. Distribution of HNO$_3$ as simulated with EMAC T106L90 at 52 hPa on certain dates between 24 December 2015 and 12 February 2016.
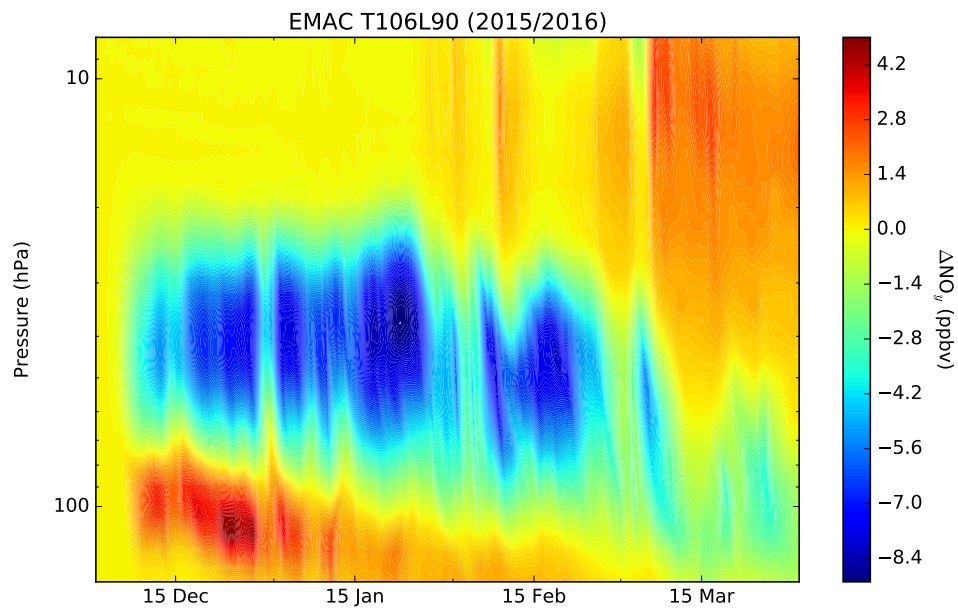
Figure 4. Redistribution of NO_y (ΔNO_y) simulated with EMAC T106L90 (difference of NO_y and the passive tracer NO_y^* ($\Delta NO_y = NO_y - NO_y^*$, averaged over 70-90°N).

EMAC T106L90 H_2O at 52 hPa
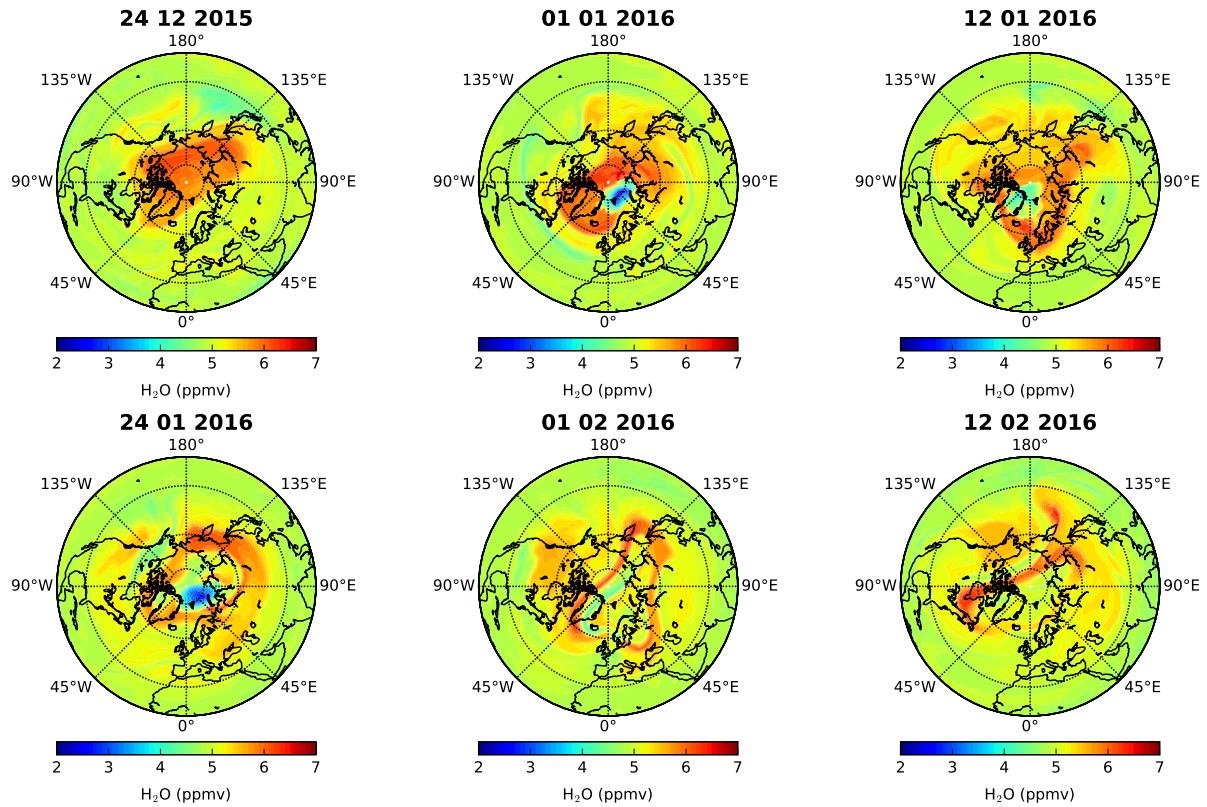
Figure 5. Distribution of H_2O as simulated with EMAC T106L90 at 52hPa on certain dates between 24 December 2015 and 12 February 2016.
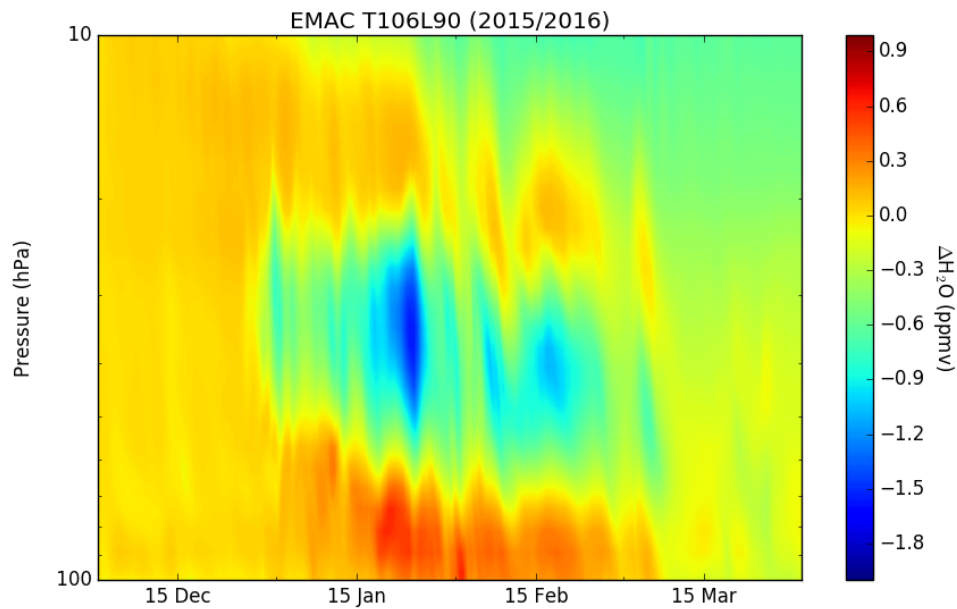
Figure 6. Redistribution of H_2O (ΔH_2O) as simulated with EMAC T106L90 at northern high latitudes (70-90°N) as function of pressure during the Arctic winter 2015/2016 (difference of total hydrogen $2CH_4+H_2O$ at time t and total hydrogen at time t_0=1 December (ΔH_2O=($2CH_4+H_2O$)(t)-($2CH_4+H_2O$)(t_0)).
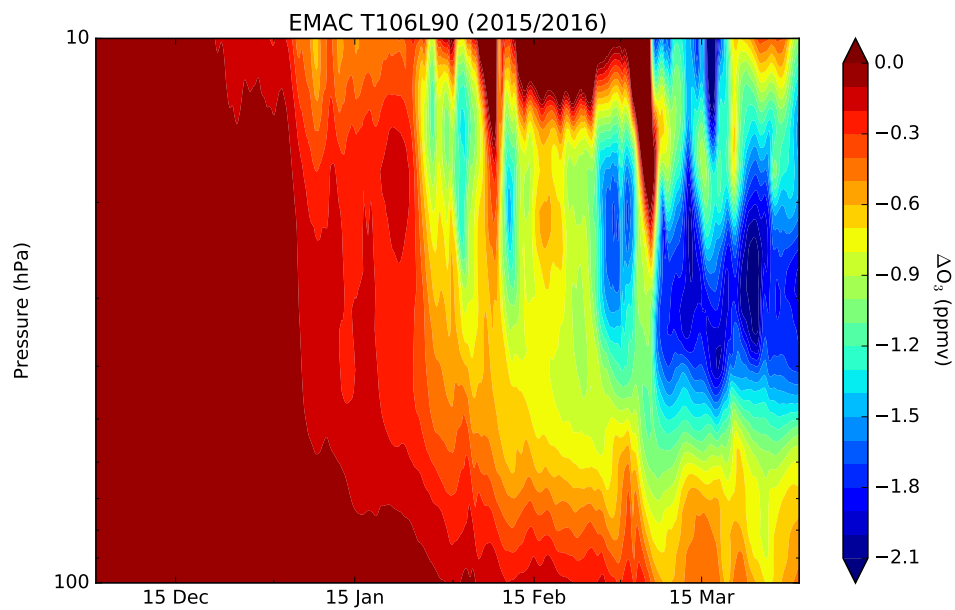
Figure 7. Ozone loss (ΔO_3) as simulated with EMAC T106L90 (difference of O_3 and the passive tracer O_3^* ($\Delta O_3 = O_3 - O_3^*$), averaged over 70-90°N) as function of time and pressure for the Arctic winter 2015/2016.
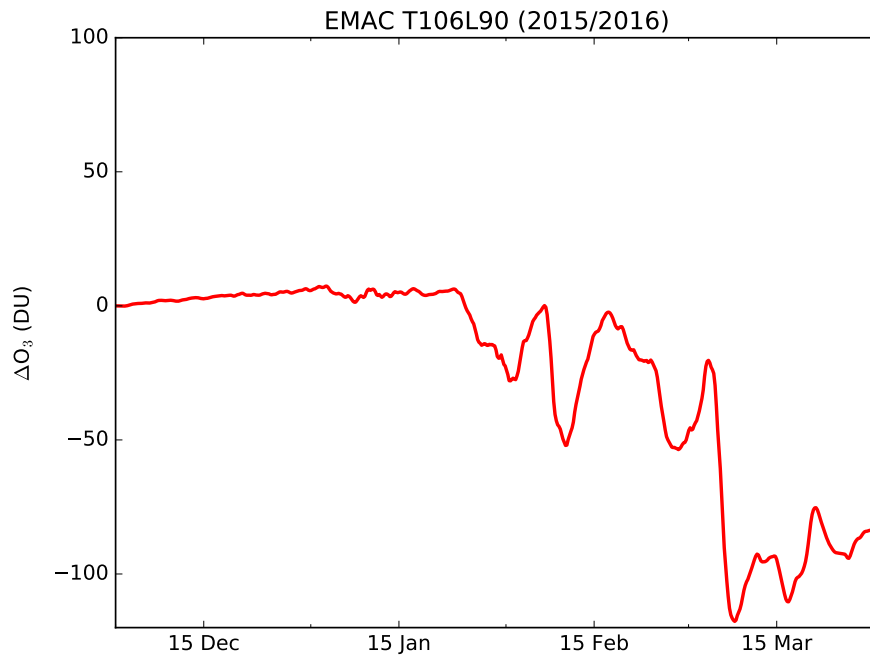
Figure 8. Total column ozone loss (ΔO_3) from EMAC T106L90 (70-90°N) for the Arctic winter 2015/2016. Total column loss has been derived from the difference between the active tracer O_3 and the passive tracer O_3^* ($\Delta O_3 = O_3 - O_3^*$).
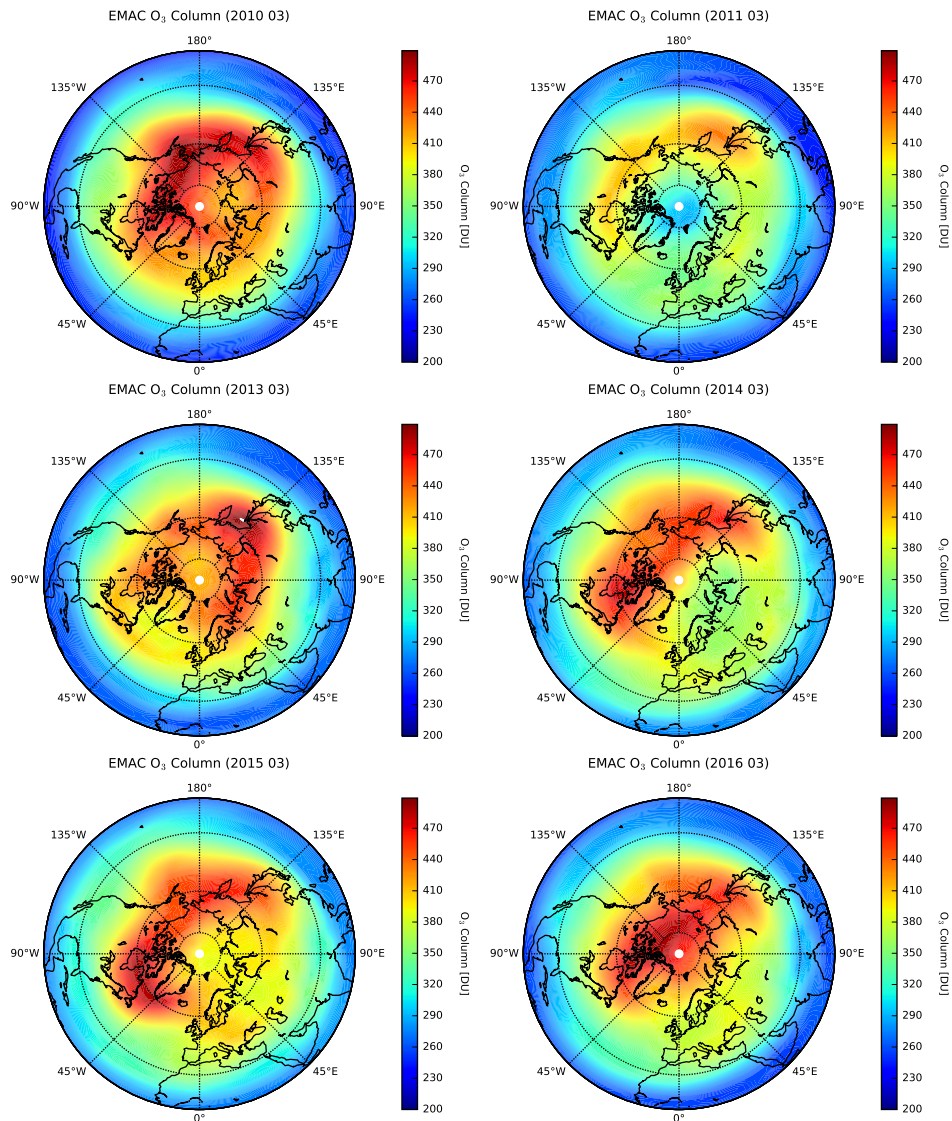
Figure 9. Total ozone column (March monthly mean) from EMAC for the years 2010-2016 (Results from the EMAC T42L90 Simulation are shown here).
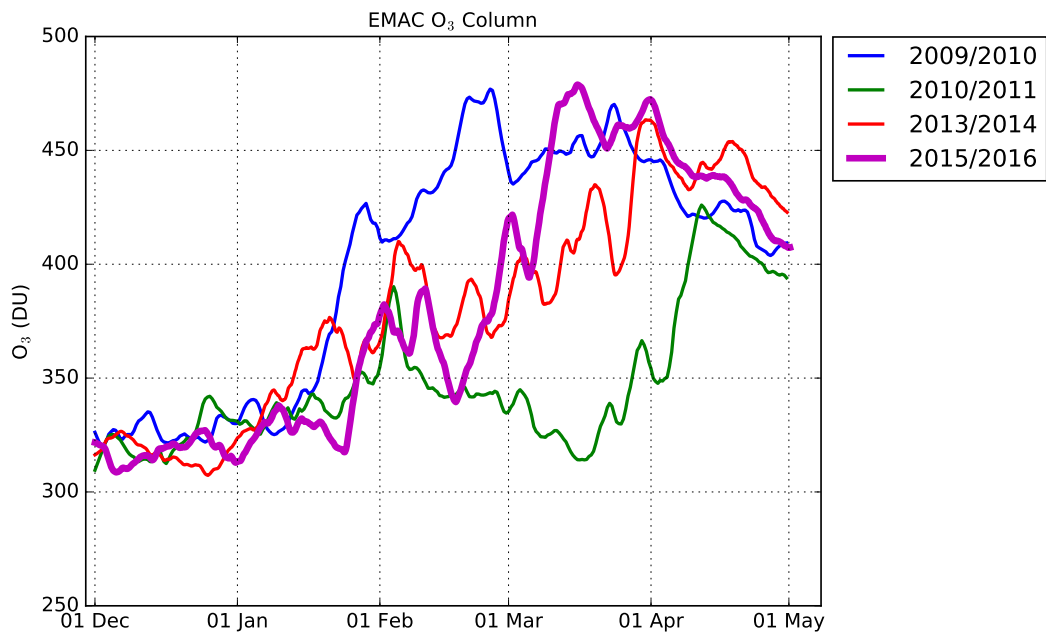
Figure 10. Ozone (O$_3$) column time series for the Arctic winters 2009/2010 (blue), 2010/2011 (green), 2013/2014 (red) and 2015/2016 (magenta) averaged over 60-90°N (Results from the EMAC T42L90 Simulation are shown here).
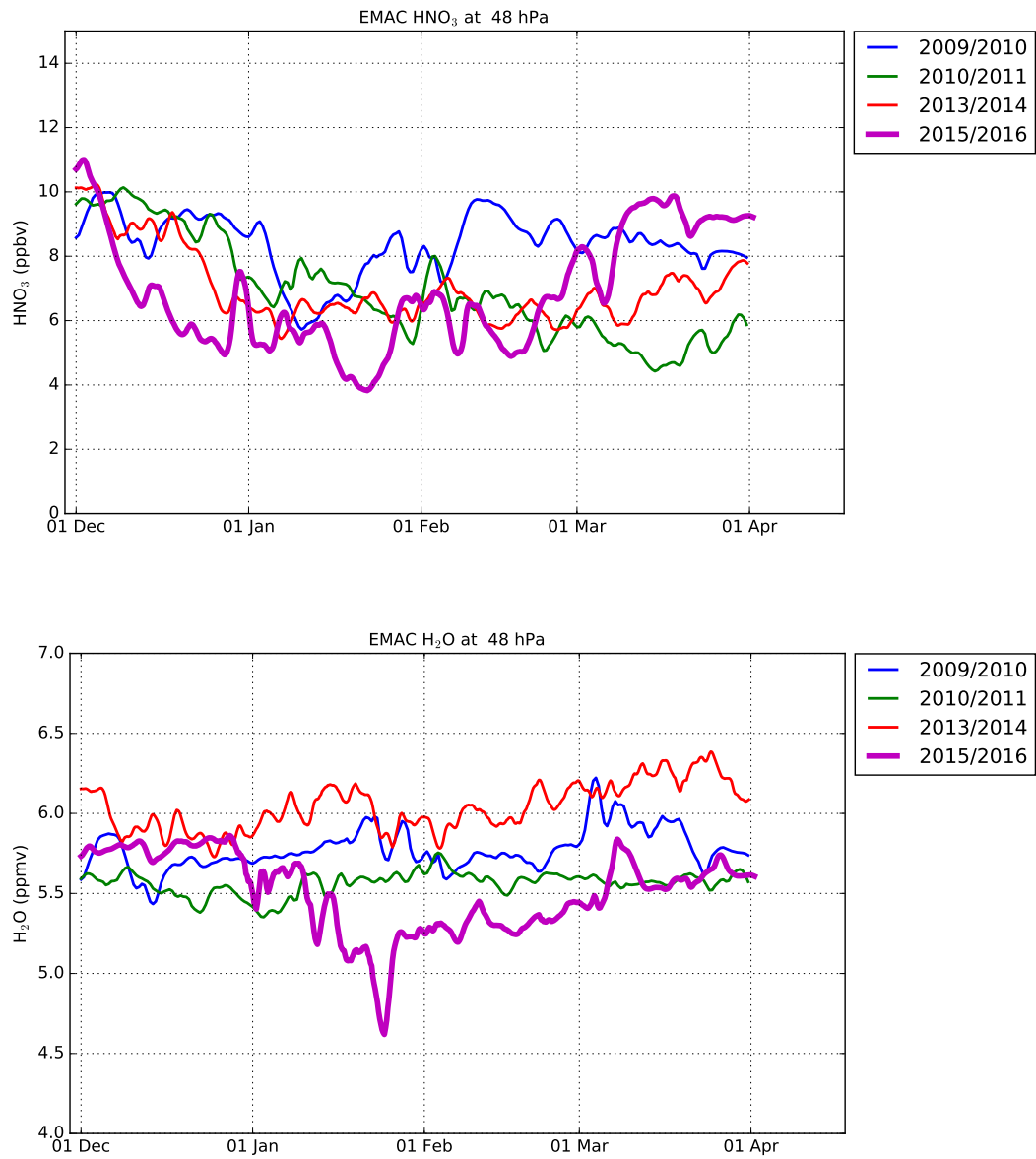
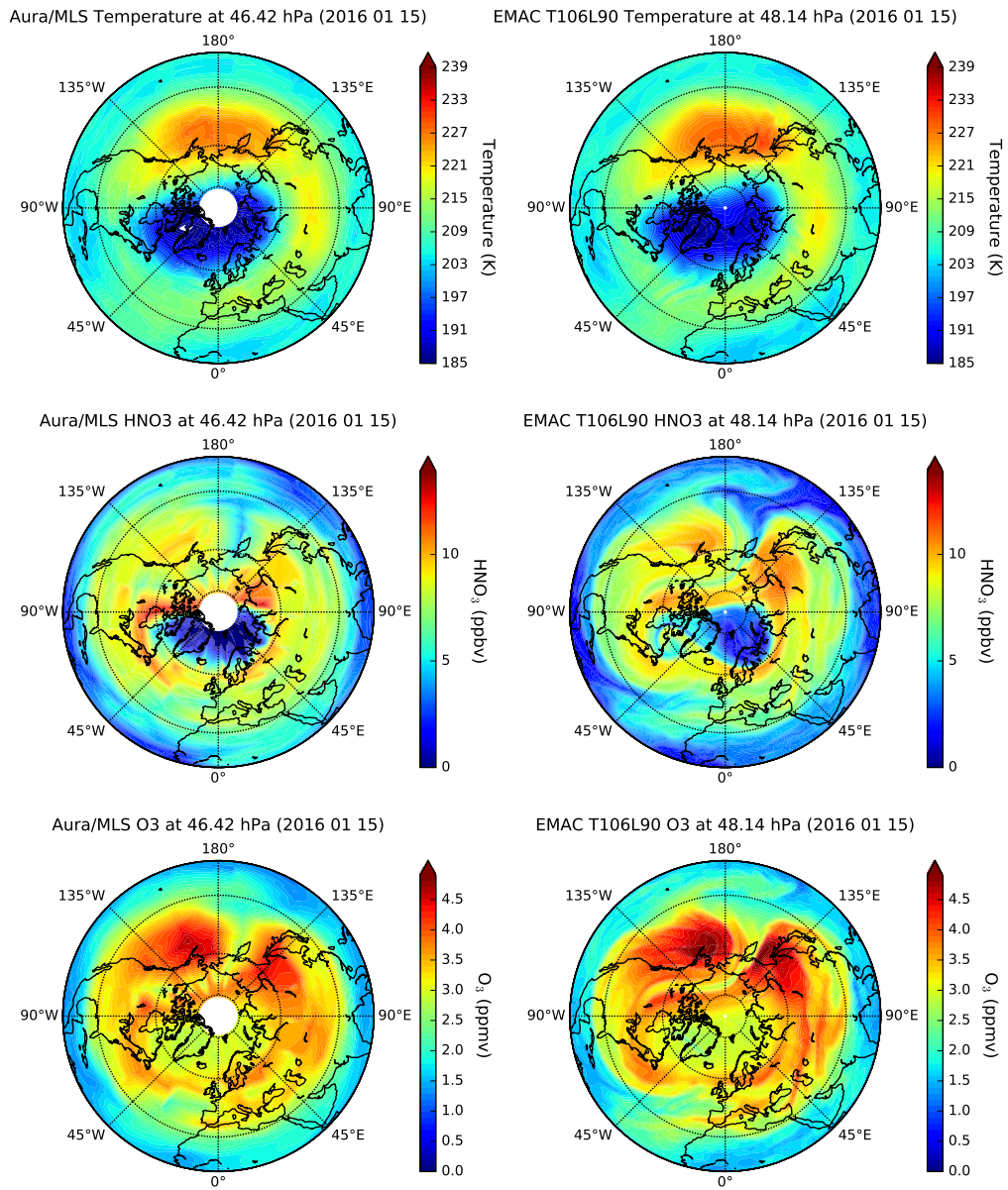**Figure 11.** Tracer time series of HNO_3 and H_2O for the Arctic winters 2009/2010 (blue), 2010/2011 (green), 2013/2014 (red) and 2015/2016 (magenta) at $48\,hPa$ averaged over $70\text{-}90°N$ (Result from the T42L90 Simulation are shown here).

Figure 12. Temperature, HNO_3, O_3 distribution measured by Aura/MLS (left) and simulated by EMAC T106L90 (right) at $\sim 50\,\mathrm{hPa}$ on 15 January 2016.
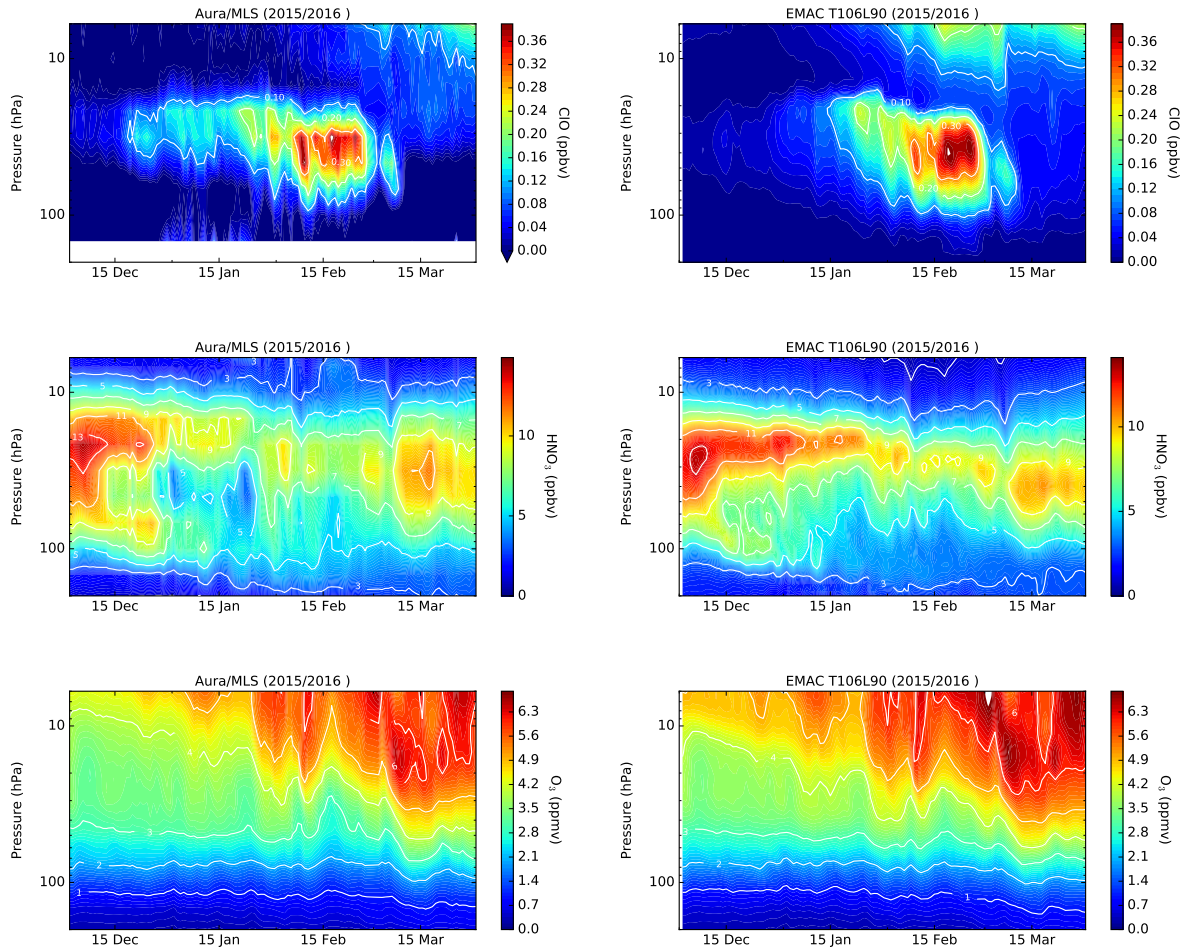
Figure 13. Temporal evolution of daily mean ClO, HNO$_3$ and O$_3$ at northern high latitudes (averaged over 70-90°N) as function of pressure as observed by Aura/MLS (left) and simulated by EMAC T106L90 (right) for the Arctic winter 2015/2016 (EMAC SORBIT output used).
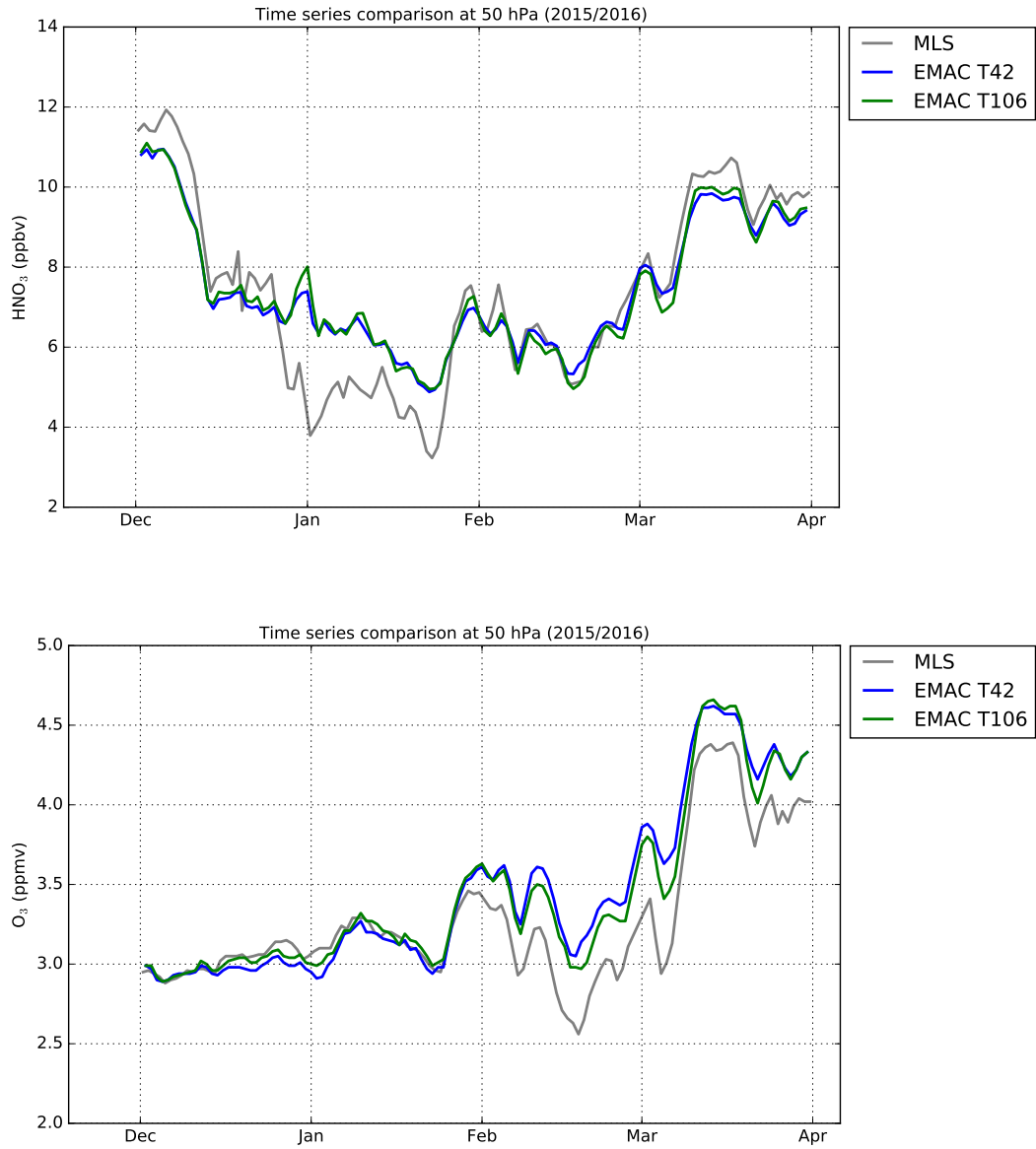
Figure 14. Time series of HNO₃ and O₃ from Aura/MLS measurements (grey) and from the EMAC T42L90 (blue), EMAC T106L90 (green) at ∼50 hPa averaged over 70-90°N (EMAC SORBIT output used).
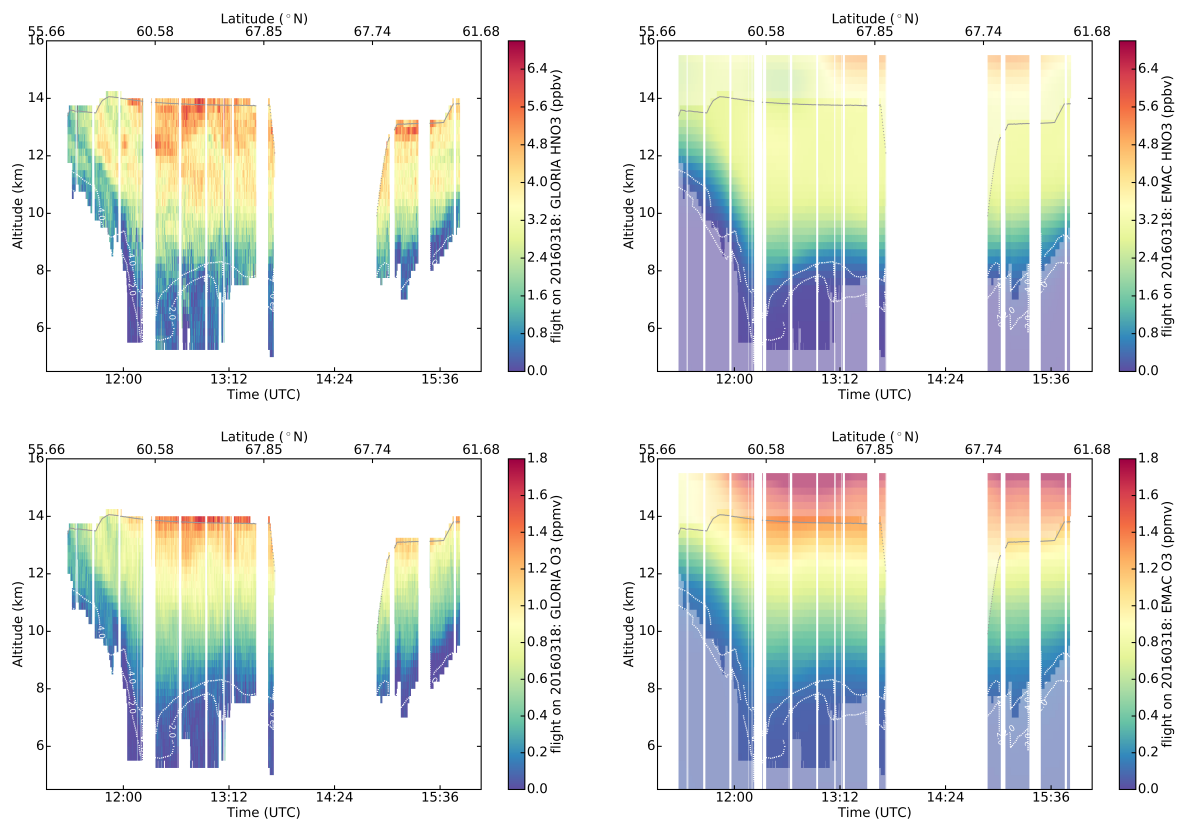
Figure 15. GLORIA HNO_3 and O_3 observations during flight 21 on 18 March 2016 (left) and EMAC T106L90 output along the flight track (right).